Diffusive dynamics of deposition-evaporation systems, jamming, and broken symmetries in related quantum-spin models

R. B. Stinchcombe and M. D. Grynberg
Department of Theoretical Physics, University of Oxford, 1 Keble Road, Oxford OX1 3NP, United Kingdom

Mustansir Barma
Department of Theoretical Physics, University of Oxford, 1 Keble Road, Oxford OX1 3NP, United Kingdom and Tata Institute of Fundamental Research, Homi Bhabha Road, Bombay 400005, India

(Received 06 January 1993)

We investigate the dynamics of models involving deposition and evaporation of dimers, trimers, ... k-mers, using analytical methods and numerical simulations. Autocorrelation functions show power-law decays in time, which are related to broken continuous symmetries in associated spin-$\frac{1}{2}$ Hamiltonians. These include the Heisenberg ferromagnet as the first nontrivial example. For $k \geq 3$ the models exhibit strongly nonergodic behavior. The numbers of both partially and fully jammed subspaces, within which the evolution takes place, increase exponentially with the size of the system. Evidence of finite-size scaling and universality over k is presented which supports a phenomenological diffusive picture for the dynamics in many subspaces.

PACS number(s): 02.50.−r, 75.10.Jm, 82.20.Mj, 05.50.+q

I. INTRODUCTION

The kinetics of processes involving the adsorption of extended objects is of interest in several physical problems, ranging from reactions on polymer chains, to chemisorption on surfaces. Here we introduce a new class of models which capture fundamental aspects of deposition and evaporation processes. The basic kinetic steps are deposition without overlap, and evaporation, possibly after recombination, of k-mers, where $k = 1, 2, 3, ...$ represent monomers, dimers, trimers, etc.

The class includes as special cases the random monomer deposition model [1] and the random dimer deposition problem of Flory [2], well known for its jammed saturation states. It also contains some features which resemble the Dickman-Burschka [3] and Bretag-Davis-Kerr-Hurst [4,5] generalizations of the random monomer problem, and of the monomer filling problem with nearest-neighbor cooperative effects, and also dimer-dimer and trimer-trimer (etc.) and other generalizations of a simplified form of catalysis models [6,7].

The class provides tractable models of nonequilibrium behavior and complex dynamics. Most of the models show strongly nonergodic behavior in which evolution takes place within separated subspaces of the total state space. The number of both fully and partially jammed subspaces is, for $k \geq 3$, exponential in the number of sites of the underlying lattice.

The models are equivalent to an interesting new class of quantum-spin models whose Hamiltonians provide the transitions described by the master equation. These spin models include noninteracting spins and isotropic Heisenberg ferromagnets as the two simplest cases. The first of these cases represents random monomer deposition and evaporation, and is special in having no cooperative effects. It is described by a simple rate equation, and shows exponential decay towards a unique steady state which is a weighted sum over all configurations. In the case of dimers, for equal deposition and evaporation rates, the Hamiltonian can be mapped into that of the isotropic Heisenberg model; for unequal rates, the Hamiltonian also has staggered fields and parity-breaking (Dzyaloshinskii-Moriya [8]) terms. An important feature of the equivalent Hamiltonians for general k-mer problems (except for monomers) is that they exhibit a continuous symmetry under spin rotations around the z axis. These continuous symmetries have, via the Goldstone theorem [9], important implications for the asymptotic dynamics.

The models have been investigated by a variety of analytic techniques, exploiting both particle and equivalent spin formulations. Some conserved quantities are readily identified in the particle picture, which also provides a natural setting for descriptions of generalized diffusion and linear response for dimer deposition and evaporation. Within the spin description, generalized spin-wave and random-walk approaches explain diffusive aspects of dynamics, while symmetry arguments may be used to infer the existence of Goldstone excitations and, in special cases, to exactly calculate time-dependent correlation functions. Jammed states may be identified in either picture, and can be enumerated by recursive techniques.

Many of the properties to be described have been discovered using numerical techniques. Large-scale Monte Carlo simulations show the long-time power-law tails characteristic of the correlation functions. The universality of diffusion behavior in all nontrivial members of the class of models is seen with large Monte Carlo simulations, and confirmed by small system Monte Carlo sim-

ulation combined with finite-size scaling analysis. This latter method provides precise values of dynamic scaling exponents and effective diffusion constants, etc. Exact enumeration algorithms have been used to study the growth of the number of subspaces with system size, to demonstrate broken ergodicity, and to estimate the degree of jamming.

Many of the points referred to above have been outlined in a recent Letter [10]. The present paper is an extended account of the work, containing essential detail necessarily absent from Ref. [10].

The layout of the remainder of this paper is as follows. Section II describes the model in detail and constructs the evolution operator in the spin representation. Section III A briefly describes the simple random monomer deposition-evaporation model and its basic properties. Section III B is an extensive discussion of the much more interesting dimer model. It begins with the special case of equal deposition and evaporation rates, which maps to the isotropic Heisenberg model. The exact correlation function and Monte Carlo results are described. The general "unequal rates" dimer case is next described and, in particular, Monte Carlo results and random-walk descriptions. Section III B continues with the generalized diffusion equation and linear response description of the dimer problem concluding with a discussion of the Flory limit and the effect of single-particle diffusion. Section IV presents an account of broken ergodicity, local jamming, and diffusive decay in the cases $k \geq 3$ (trimers, etc.) where numbers of subspaces — both fully jammed and partially jammed — are shown to be exponential in site number. A quantitative measure of jamming is also provided. Monte Carlo evidence for diffusive decay is presented and interpreted in terms of random walks of patches of active sites on jammed backgrounds. Section V treats in turn conserved quantities, symmetries and Goldstone bosons, which provide an explanation of the slow asymptotic kinetics. Section VI provides the evidence for universal k-independent diffusion behavior from finite-size scaling as well as a calculation of the finite-size scaling function. Section VII is a concluding summary and further outlook. Detailed analyses are relegated to appendixes on (A) coverage in steady state for dimers, (B) calculation of the autocorrelation function for dimers with equal rates, (C) recursive evaluation of numbers of fully jammed states, (D) a random walk of spin flips in a jammed trimer configuration.

II. THE MODEL AND ITS EVOLUTION OPERATOR

Let us consider a d-dimensional lattice on which k nearest-neighbor sites are selected at random. The basic process under consideration in this work involves deposition and evaporation of k-mers, where $k = 1, 2, 3, \ldots$ denotes monomers, dimers, trimers, etc. Deposition attempts occur with rate ϵ at selected locations and are successful only if k adjacent sites are vacant. Additionally, evaporation of k particles at a time occurs at rate ϵ', provided of course that all the k selected lattice sites are indeed already occupied. These microscopic dynamical rules are schematized in Fig. 1 for the case of a linear chain.

It is worthwhile to point out that during this process, the hard-core character of the particles and the possibility of evaporation give rise to the reconstruction of k-mer groups and redistribution of particles. Thus, although our model contains no explicit particle hopping terms, it allows for an effective particle diffusion.

Our study is mainly limited to one-dimensional systems for two reasons. Firstly, fluctuation effects are strongest in $d = 1$, and already the case of linear k-mers on a chain displays a very rich behavior. Secondly, with modern computer facilities numerical simulations of sufficiently high quality are possible in $d = 1$; our results were obtained with $k = 2, 3, 4$.

The time dependence of this kinetic model is described, as usual, by a master equation [11] which governs the time evolution of the probabilities of finding a certain particle configuration at time t. The associated time evolution operator H is expressed in terms of Pauli matrices and thus describes a quantum spin-$\frac{1}{2}$ problem. In this work we shall explore the connections between these two types of problems and show what can be learned in that way.

Consider a linear chain of Ising spins $s_l = \pm 1$, $l = 1, 2, \ldots, L$. The presence of a particle (vacancy) at site l is represented by $s_l = +1$ (-1). Let $|\, s \,\rangle = |s_1, s_2, \ldots, s_L\,\rangle$ denote a particle configuration of the lattice which we assume to have cyclic boundary conditions, $s_{L+1} \equiv s_1$.

If $P(s,t)$ denotes the probability of finding a configuration $|s\rangle$ at time t and $W(s \to s')$ represents the rate or transition probability per unit time at which configuration $|s\rangle$ evolves to $|s'\rangle$, the master equation is

$$\frac{\partial}{\partial t} P(s,t) = \sum_{s'} \Big[W(s' \to s)\, P(s',t) - W(s \to s')\, P(s,t) \Big] . \tag{1}$$

The basis vectors $|\, s \,\rangle$ (diagonal in the $|\, \{\sigma_l^z\} \,\rangle$ representation, say) are orthonormal and complete, $\langle s|s'\rangle = \delta_{s,s'}$, $\sum_s |s\rangle\langle s| = \mathbf{1}$, hence a state with probability $\{P(s,t)\}_s$ is represented in this space by a vector $|P(t)\rangle$ defined by

$$|\, P(t) \,\rangle = \sum_s P(s,t)\, |\, s \,\rangle . \tag{2}$$

The master equation (1) can now be written as

$$\frac{\partial}{\partial t} |\, P(t) \,\rangle = -\, H\, |\, P(t) \,\rangle , \tag{3}$$

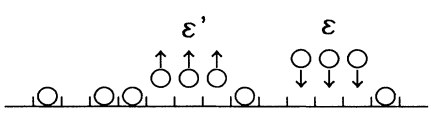

FIG. 1. Schematic view of the deposition-evaporation process for trimers on a linear chain.

where the operator H is defined in terms of its matrix elements, namely,

$$\langle s' \,|\, H \,|\, s \rangle = -W(s \to s') \quad , \quad s' \neq s \,,$$
$$\langle s \,|\, H \,|\, s \rangle = \sum_{s' \neq s} W(s \to s') \,. \tag{4}$$

Evidently, through a single elementary deposition-evaporation process, the state $|s\rangle$ can evolve to $|s'\rangle$ only if $|s\rangle$ differs from $|s'\rangle$ in a *single* group of k nearest-neighbor parallel spins at locations $l, l+1, \ldots, l+k-1$, say. The corresponding rates are given by

$$|\, s_1, \ldots, \downarrow_l, \ldots, \downarrow_{l+k-1}, \ldots, s_L \,\rangle$$
$$\to |\, s_1, \ldots, \uparrow_l, \ldots, \uparrow_{l+k-1} \ldots, , s_L, \,\rangle \,, \quad W(s \to s') = \epsilon$$
$$|\, s_1, \ldots, \uparrow_l, \ldots, \uparrow_{l+k-1}, \ldots, s_L \,\rangle$$
$$\to |\, s_1, \ldots, \downarrow_l, \ldots, \downarrow_{l+k-1}, \ldots, s_L \,\rangle \,, \quad W(s \to s') = \epsilon' .$$

Therefore the operator H connects $|s\rangle$ with $|s'\rangle$ through two terms of the form $\epsilon\, \sigma_l^+, \ldots, \sigma_{l+k-1}^+ + \epsilon'\, \sigma_l^-, \ldots, \sigma_{l+k-1}^-$, where σ_l^+ (σ_l^-) is a spin-$\frac{1}{2}$ raising (lowering) operator at site l. Consequently, to take into account an arbitrary k-mer location and reproduce the matrix elements of Eq. (4), the nondiagonal part of H should be of the form

$$H - \sum_s \left(\sum_{s' \neq s} W(s \to s') \right) |\, s \,\rangle \langle\, s \,| = -\sum_n Q_n \,,$$
$$Q_n = \epsilon \prod \sigma_l^+ + \epsilon' \prod \sigma_l^- \,, \tag{5}$$

where $\prod \equiv \prod_{l=n}^{n+k-1}$.

Let us now consider the diagonal matrix elements of Eq. (4). From the above discussion it is clear that $\langle s \,|\, H \,|\, s \rangle$ is proportional to the total number of ways in which configurations $|s\rangle$ can evolve to different states $|s'\rangle$ in a *single* elementary deposition-evaporation process. For instance, the total number of successful deposition attempts on state $|s\rangle$ are counted by the operator

$$\hat{\mathcal{N}}_{\rm dep} = \sum_n \prod \left(1 - \sigma_l^+ \sigma_l^- \right) , \tag{6}$$

namely, the number of k contiguous down spins (vacant sites). Similarly, the total number of successful evaporation attempts are taken into account by

$$\hat{\mathcal{N}}_{\rm ev} = \sum_n \prod \sigma_l^+ \sigma_l^- \,, \tag{7}$$

which yields the number of k adjacent up spins (occupied sites) of state $|s\rangle$. Therefore we get

$$\sum_{s' \neq s} W(s \to s') = \langle\, s \,|\, \epsilon \hat{\mathcal{N}}_{\rm dep} + \epsilon' \hat{\mathcal{N}}_{\rm ev} \,|\, s \,\rangle \,. \tag{8}$$

Recalling Eqs. (5) and (8) and noting that $\sigma_l^z = 2\sigma_l^+ \sigma_l^- - 1$, we finally conclude that the operator governing the time evolution of our deposition-evaporation model should have the form

$$H = \sum_n \left(R_n - Q_n \right) ,$$
$$R_n = \epsilon \prod \tfrac{1}{2} \left(1 - \sigma_l^z \right) + \epsilon' \prod \tfrac{1}{2} \left(1 + \sigma_l^z \right) . \tag{9}$$

It is worthwhile to remark that the columns of H satisfy $\sum_{s'} \langle s'|H|s\rangle \equiv 0$, as is required by conservation of probability.

Formal integration of Eq. (3) yields the stochastic evolution operator of our problem $U(t, t_0) = \exp\left[-H \left(t - t_0 \right) \right]$

$$|\, P(t) \,\rangle = U(t, t_0) \,|\, P(t_0) \,\rangle \,. \tag{10}$$

Note that H has a non-negative spectrum [11] because no probability can grow with time. The steady states of our kinetic model correspond to the ground states with eigenvalue $E_0 = 0$ of each of the invariant subspaces of H. Positive eigenvalues $E > 0$ correspond to eigenstates decaying with a lifetime $1/E$.

In general H connects states only within disconnected subspaces of the total state space. Many of these subspaces contain only a single state, namely, there are particular configurations which cannot change or evolve under the action of H; we will refer to them as fully "jammed" states. The concept of jamming in our model, i. e., the impossibility to deposit or evaporate k-mers due to the absence of k contiguous vacant or occupied sites, can in fact be quantified in terms of a transition probability current in the steady state, giving rise to the idea of partially jammed states. It will turn out, that on "nearly" jammed subspaces an exact solution is possible. These ideas will be developed in full detail in Secs. III and IV.

In the Ising or particle representation, a set of independent constants of motion can be easily identified. Assuming that the number of sites L in the lattice is a multiple of k, we can divide the chain into k sublattices $\alpha = 1, 2, \ldots, k$ such that a given site l belongs to sublattice α if $l = k\,Z + \alpha$ where Z is an integer. For any state $|\, s \,\rangle$ define $\mathcal{N}_\alpha \equiv \sum_{l \in \alpha} \sigma_l^+ \sigma_l^- \,|\, s \,\rangle$ as the total occupation of sublattice α. Clearly the deposition-evaporation process preserves $\mathcal{N}_\alpha - \mathcal{N}_\beta$ since at any time the number of incoming or outgoing particles on each sublattice is the same (see Fig. 1). Therefore the dynamics conserves $M_\alpha - M_\beta$ where $M_\alpha = 2\mathcal{N}_\alpha - L/k$ is the corresponding sublattice magnetization. Hence there are $k-1$ independent quantities of this type. It is worth pointing out that this family of conservation laws can also be derived on more general grounds by considering the continuous symmetries of the evolution operator H, as will be discussed in Sec. V. Most of the H-invariant subspaces

have nonzero values of $M_\alpha - M_\beta$ implying broken translational invariance or an inhomogeneous distribution of particles in the corresponding steady state.

It is useful to construct alternative representations of H. Let us introduce the operators $\xi_l \equiv \gamma\,\sigma_l^+ + \gamma^{-1}\,\sigma_l^-$, which arise from a "pseudorotation" (i. e., rotations with a pure imaginary argument) of the original spins. It can be checked out easily that

$$H = \sum_n R_n \left(1 - \prod \xi_l\right), \tag{11}$$

provided that $\gamma = (\epsilon/\epsilon')^{1/k}$. Furthermore, since the eigenvalues of ξ_l are $m_l = \pm 1$, it is clear that product eigenstates of ξ_l such that $\prod_{l=n}^{n+k-1} m_l = 1$ with $1 \le n \le L$ are indeed steady states, from which many more can be generated by exploiting symmetries of H (Sec. V). However, they arise from linear combinations of steady states belonging to each subspace and therefore do not have a simple interpretation in the σ^z representation given so far.

It is also possible to rewrite the time evolution generator H in terms of k-mer creation and annihilation operators $A^\dagger$, A

$$A_n^\dagger \equiv \prod \sigma_l^+ \quad , \quad A_n \equiv \prod \sigma_l^- . \tag{12}$$

Using the spin commutation rules $[\,\sigma_i^+\,,\,\sigma_j^-\,] = \delta_{i,j}\,\sigma_i^z$ and $\{\,\sigma_l^+\,,\,\sigma_l^-\,\}_+ = 1$, H adopts the suggestive form

$$\begin{aligned} H &= \sum_n \left(\epsilon'\,A_n^\dagger\,A_n + \epsilon\,A_n\,A_n^\dagger - \epsilon\,A_n^\dagger - \epsilon'\,A_n\right) \\ &\equiv \sum_n U_n . \end{aligned} \tag{13}$$

For $k = 2$ and $\epsilon = \epsilon'$, the operators U_n satisfy the requirements of a Temperley-Lieb algebra [12] allowing an exact solution of the dynamical correlation functions. This case will be analyzed in detail in Appendix B, although from a different approach. Unfortunately, the more complex and interesting cases only satisfy two of the three requirements for such an algebra.

III. MONOMERS AND DIMERS: SPIN AND PARTICLE DESCRIPTIONS

A. Monomers

For the case of monomers ($k = 1$) the evaporation-deposition process is very simple. There are no cooperative effects [13], so it can be described by simple rate equations. For example, the coverage ρ (average particle occupation per site) satisfies

$$\frac{d\rho}{dt} = \epsilon\,(1-\rho) - \epsilon'\,\rho . \tag{14}$$

The coverage therefore decays exponentially in time to a steady state value $\epsilon/(\epsilon+\epsilon')$. There is no jamming in this case.

In preparation for less trivial examples, it is helpful to see how the above results arise in the spin description of the monomer case. Here the stochastic evolution operator takes the following noninteracting form:

$$\begin{aligned} H &= \sum_l \left[\,\tfrac{1}{2}\,\epsilon\,(1-\sigma_l^z) + \tfrac{1}{2}\,\epsilon'\,(1+\sigma_l^z) - \epsilon\,\sigma_l^+ - \epsilon'\,\sigma_l^-\,\right] \\ &= \sum_l \left[\,\tfrac{1}{2}\,\epsilon\,(1-\sigma_l^z) + \tfrac{1}{2}\,\epsilon'\,(1+\sigma_l^z)\,\right](1-\xi_l) , \end{aligned} \tag{15}$$

where $\xi_l \equiv (\epsilon/\epsilon')\,\sigma_l^+ + (\epsilon'/\epsilon)\,\sigma_l^-$. Hence for $\epsilon = \epsilon'$ we have $H = \epsilon \sum_l (1 - \sigma_l^x)$. Thus for equal rates of deposition and evaporation the eigenstates have $\sigma_l^x = \pm 1$. Among these, there is one state with zero eigenvalue E, namely, the state with $\sigma_l^x = 1$ for all sites l. This corresponds to the unique steady state $|\,\psi_0\,\rangle$

$$|\,\psi_0\,\rangle = \prod_{l=1}^{L} \frac{1}{\sqrt{2}}\,(\,|\uparrow\rangle_l + |\downarrow\rangle_l\,) . \tag{16}$$

All other eigenstates have some σ_l^x equal to -1 and their eigenvalues are a positive integer multiple of ϵ. These gaps correspond to the inverse characteristic time of exponential decay.

For $\epsilon \neq \epsilon'$ it can be seen that corresponding statements apply with "rotated" spins. From the second form of H [Eq. (11)] we see that the steady state is a coherent superposition of spin-up and spin-down, i. e., of particle and vacancy (at each site l), with relative weights ϵ, ϵ', as already known from the particle picture.

B. Dimers

Cooperative effects occur for all $k \ge 2$ (dimers, trimers, etc.). The simplest case is that of dimers and has further simplifications for equal deposition and evaporation rates. The general dimer Hamiltonian ($\epsilon \neq \epsilon'$) is obtained by inserting $k = 2$ in Eq. (9). The result involves spin-pair-interaction terms. It is easy to see that the deposition term $\sum_l \sigma_l^+\,\sigma_{l+1}^+$ and the evaporation term $\sum_l \sigma_l^-\,\sigma_{l+1}^-$ have no effect on the two Néel states, in which σ_l^z takes the value $(-1)^l$ [or $(-1)^{l+1}$]. As a consequence the remaining detailed balance terms in H have no effect on these states. They are "fully jammed" steady states.

The following spin rotation is suggested:

$$\boldsymbol{\tau}_l = R_l\,\boldsymbol{\sigma}_l\,R_l^{-1} \quad , \quad R_l = \exp\left(-i\,\frac{\pi}{2}\,l\,\sigma_l^x\right) , \tag{17}$$

therefore $(\,\tau_l^x,\,\tau_l^y,\,\tau_l^z\,) = (\,\sigma_l^x,\,(-1)^l\,\sigma_l^y,\,(-1)^l\,\sigma_l^z\,)$. This sublattice mapping takes the Hamiltonian to the form

$$\mathcal{H} = \frac{\epsilon' - \epsilon}{2} \sum_l (-1)^l \left(\tau_l^z + \tau_l^+ \tau_{l+1}^- - \tau_l^- \tau_{l+1}^+ \right) + \frac{\epsilon' + \epsilon}{4} \sum_l \left(1 - \boldsymbol{\tau}_l \cdot \boldsymbol{\tau}_{l+1} \right) . \tag{18}$$

In addition to an isotropic Heisenberg coupling, $\mathcal{H}$ contains staggered field and Dzyaloshinskii-Moriya terms [8]. Evidently, $\mathcal{H}$ commutes with $T^z \equiv \sum_l \tau_l^z$. In a system with L sites, T^z runs over $(L+1)$ values, implying that $\mathcal{H}$ splits into as many invariant subspaces. The subspace with r down spins ($T_z = L - 2r$) contains $\binom{L}{r}$ configurations $|C_r\rangle$. Using detailed balance, the corresponding (unnormalized) steady state is seen to be

$$|\psi_r^0\rangle = \sum_{|C_r\rangle} \epsilon^{N_A(C_r)} \epsilon'^{N_B(C_r)} |C_r\rangle \tag{19}$$

where $N_A(C_r), N_B(C_r)$ are the numbers of particles in sublattices A and B in a particular configuration $|C_r\rangle$.

The coverage Θ_0 in the steady state (Appendix A), defined as the mean number of occupied sites in the dimer problem, is given by

$$\Theta_0 = \frac{1}{2} \left(1 + \frac{\langle T_A \rangle - \langle T_B \rangle}{L} \right) \tag{20}$$

where $T_A^z \equiv \sum_{l \in A} \tau_l^z$, $T_B^z \equiv \sum_{l \in B} \tau_l^z$. Since the steady state in each subspace (labeled by the value of T^z) is known explicitly [Eq. (19)], the corresponding values of $\langle T_A \rangle$, $\langle T_B \rangle$ and Θ_0 can be found, for each T^z. In particular, for the subspace $T^z = 0$ (which includes the all-empty configuration in the initial dimer problem) the result (see Appendix A for calculational details) is

$$\Theta_0 = \frac{1}{1 + \sqrt{\epsilon'/\epsilon}} \tag{21}$$

1. *Dimers, $\epsilon = \epsilon'$*

For equal deposition and evaporation rates the new form of dimer Hamiltonian reduces to that for the isotropic ferromagnetic Heisenberg chain

$$\mathcal{H} = -\frac{\epsilon}{2} \sum_l \left(\boldsymbol{\tau}_l \cdot \boldsymbol{\tau}_{l+1} - 1 \right) . \tag{22}$$

The ground states with all spins τ_l^z up, or all down, correspond to the fully jammed zero energy states discussed above. More generally, because of the isotropic nature of the interaction term in $\mathcal{H}$, there are $L+1$ ground states ($E = 0$) with all spins $\boldsymbol{\tau}_l$ parallel — each a steady state.

$\mathcal{H}$ is invariant under common rotation of all spins $\boldsymbol{\tau}_l$. The operator producing such a rotation about an axis parallel to an arbitrary unit vector $\mathbf{n}$ is $\mathbf{T} \cdot \mathbf{n}$ where $\mathbf{T} = \sum_l \boldsymbol{\tau}_l$. So $[\mathbf{T}, \mathcal{H}] = 0$, and each component of $\mathbf{T}$ is conserved in the deposition-evaporation process ($k = 2$, $\epsilon = \epsilon'$). As we have seen, $\mathcal{H}$ commutes with T^z even if the deposition and evaporation rates ϵ and ϵ' are different. But the commutation with T^x and T^y (and hence with the total spin $\hat{T}^2 \equiv T^{x\,2} + T^{y\,2} + T^{z\,2}$) is a special feature of the model with $\epsilon = \epsilon'$.

A parallel-spin steady state $|G\rangle_{T^z}$ with specified value of T^z (i.e., with given number of τ particles, namely the particles in the sublattice mapped system) can be obtained by rotating the fully jammed states $|G\rangle_L$ with all L spins up by applying $T^- \equiv T^x - iT^y$ an appropriate number $r \equiv (L - T^z)/2$ of times. $|G\rangle_{T^z}$ is a sum over all states of the specified particle number with equal coefficients; each such configuration is equally likely in the steady state.

It is well known that the isotropic ferromagnetic Heisenberg model has single spin-wave excited states. For specified T^z and wave vector q, these are obtained by applying to $|G\rangle_{T^z+1}$ the spin-rotated version of the qth Fourier component of the spin lowering operator $T_q^- \equiv L^{-1/2} \sum_l \tau_l^- \exp(iql)$. The spin waves have a gapless spectrum with excitation energy (i.e., the eigenvalues E of our $\mathcal{H}$) proportional to q^2 at small wave vector q: $E = E_q \equiv \epsilon(1 - \cos q) \simeq D q^2$ for small q. This form applies for spin-wave excitations from any of the parallel-spin steady states, and the spin-wave stiffness constant D is the same ($D = \epsilon/2$) for all such states.

The gapless character of the spin-wave band has important implications for the asymptotic kinetics for dimer deposition and evaporation with $\epsilon = \epsilon'$. It is well known that the spin-wave contribution to the spin autocorrelation function $\langle \tau_l^z(t)\, \tau_l^z(0) \rangle - \langle \tau_l^z \rangle^2$ in the all-up-spin ground state ($T^z = L$) has a diffusive $t^{-1/2}$ long-time tail. As a consequence of the full rotational symmetry of $\mathcal{H}$ the autocorrelation function in the steady state with average τ particle occupation $\tilde{\rho} = \frac{1}{2}(1 + \langle T^z \rangle / L)$ can also be calculated exactly. Simple selection rules arising from this symmetry apply to the matrix elements of τ_l^z in the basis of eigenstates of $\mathcal{H}$. This simplifies significantly the calculation of dynamical correlation functions, which is given in detail in Appendix B for the sake of completeness. The final result turns out to be

$$\begin{aligned} C(t) &\equiv \frac{1}{L} \sum_l \left[\langle n_l(t)\, n_l(0) \rangle - \langle n_l \rangle^2 \right] \\ &= \tilde{\rho}\,(1 - \tilde{\rho}\,) \frac{1}{L} \sum_q \exp(-E_q t) \\ &= \tilde{\rho}\,(1 - \tilde{\rho}\,) \exp(-2\epsilon t)\, I_0(2\epsilon t) \propto t^{-\frac{1}{2}} , \quad t \to \infty , \\ I_0(z) &\equiv \frac{1}{2\pi} \int_{-\pi}^{\pi} \exp(z \cos\theta)\, d\theta . \end{aligned} \tag{23}$$

This prediction of a diffusive power-law asymptotic kinetics contrasts with the exponential decay of the monomer case. The diffusive tail is intuitively surprising given that the model has no explicit diffusion process, but as remarked earlier the reconstitution of k-mers on the surface does result in effective particle diffusion.

Monte Carlo simulations have been used to investigate this phenomenon. The simulation procedure goes as follows. Using periodic boundary conditions we choose a lattice site at random and check out if there are either

$k-1$ consecutive vacant or occupied sites to the right of the selected site. If the selected site is empty and its $k-1$ contiguous neighbors are also vacant, a k-mer deposition is attempted with probability ϵ. Similarly, a k-mer evaporation attempt with probability ϵ' is allowed provided that the corresponding sites are already occupied. If neither deposition nor evaporation is possible, the selected site remains in its occupation number state. This microprocess is repeated L times after which the time is increased by one unit ($t \to t+1$). Therefore the time is defined proportional to the number of deposition-evaporation attempts (successful or not).

Starting from an all empty initial configuration (actually belonging to the least jammed subspace for $\epsilon = \epsilon'$), we waited a time t_0 to allow the system to reach the stationary regime. In general t_0 was chosen larger than the subspace dependent relaxation time of the full system. Using t_0 as the time origin we measured the autocorrelation function of Eq. (23) in the steady state by averaging over different histories.

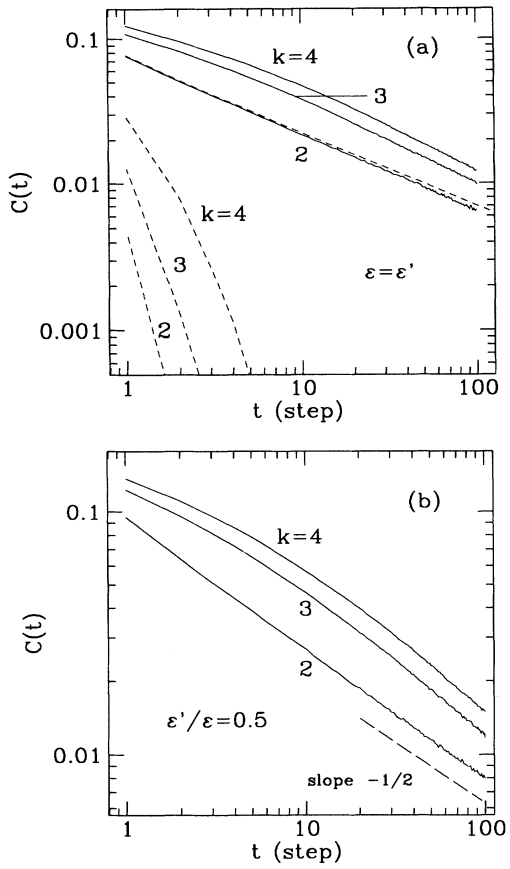

FIG. 2. Autocorrelation function in the steady state obtained from an empty lattice of $L = 1.2 \times 10^5$ sites, averaged over 100 samples for $k = 2, 3, 4$ indicating a power-law decay ($\sim t^{-1/2}$). (a) Results for $\epsilon = \epsilon'$. The analytic determination for $k = 2$ [Eq. (23) in the text] is shown by the dashed curve. Explicit particle diffusion results in an exponential decay (dashed curves at the bottom left). (b) Results for $\epsilon'/\epsilon = 0.5$.

We used chains of $L = 1.2 \times 10^5$ sites with periodic boundary conditions. On general grounds we expect spatial correlations to be insignificant for separations comparable to the linear dimension of the system, hence finite-size effects can be assumed to be negligible. The averages were taken over 100 histories using $t_0 = 5000$ steps on each sample. The results for $\epsilon = \epsilon'$ are shown in Fig. 2(a) along with the more complex cases $k = 3$ and 4 to be referred to in the remaining sections. They are consistent with Eq. (23) (dashed line). At long times, the decay follows a power law ($\sim t^{-1/2}$), a feature which evidently also characterizes the decay for $k = 3$ and 4 as well.

2. *Dimers, $\epsilon \neq \epsilon'$*

For unequal deposition-evaporation rates, the dimer spin Hamiltonian takes the general form given in Eq. (18). Monte Carlo simulations of the autocorrelation function for this case again exhibit power-law asymptotic decay, despite the lack of isotropy in the Hamiltonian. This is shown in Fig. 2(b) for $\epsilon'/\epsilon = 0.5$. This behavior is rather fully explained in the following subsection, using an effective diffusion equation in the particle picture, and in Sec. V using hidden symmetries of the Hamiltonian.

We now give a simple "random-walk" description which applies (for general ϵ, ϵ') to the particular case $(\tilde{\rho}_A, \tilde{\rho}_B) \sim (1,1)$, i.e., "near" the two fully jammed states. Suppose $|0\rangle$ denotes the fully jammed state with all spins up ($\tilde{\rho} = 1$) in the sublattice representation. Then the single-spin-flip state $|n\rangle = \tau_n^- |0\rangle$ evolves as follows under the action of $\mathcal{H}$ [Eq. (18)]:

$$\mathcal{H}|2n\rangle = b\,(1+a)\,(|2n+1\rangle - 2|2n\rangle + |2n-1\rangle)\,, \tag{24}$$

$$\mathcal{H}|2n+1\rangle = b\,(1-a)\,(|2n+2\rangle - 2|2n+1\rangle + |2n\rangle)\,,$$

where $a \equiv (\epsilon - \epsilon')/(\epsilon + \epsilon')$ and $b \equiv (\epsilon + \epsilon')/2$.

These equations for the random walk of the spin flip have a form consistent with conservation of probability and with translational invariance on each of the two sublattices. Hence the substitutions $|2n\rangle \propto \alpha \exp(iq\,2n)$, $|2n+1\rangle \propto \beta \exp[iq(2n+1)]$ reduce these equations to the form $\mathcal{H}|q\rangle = E_q|q\rangle$. The eigenenergies and eigenvectors are

$$E_q = 2b\left(1 \pm \sqrt{\cos^2 q + a^2 \sin^2 q}\,\right),$$
$$|q\rangle = A_q|0\rangle \equiv \sum_n \exp(iq\,2n)\left(\alpha\tau_{2n}^- + \beta\exp(iq)\,\tau_{2n+1}^-\right)|0\rangle, \tag{25}$$
$$\frac{\beta}{\alpha} = \frac{2b(1+a)\cos q}{E_q + 2b(1-a)}\,.$$

The resulting gapless ("acoustic") mode has $E_q \sim D q^2$, $q \to 0$ with

$$D = \frac{\epsilon \epsilon'}{\epsilon + \epsilon'} . \tag{26}$$

This is sufficient to give the $t^{-1/2}$ decay for $(\tilde{\rho}_A, \tilde{\rho}_B) \sim (1,1)$. The procedure also generates another steady state $A_0 \,|\, 0 \rangle$ in addition to the jammed state.

An alternative procedure, leading to equivalent results, is to find α_n, β_n and E such that

$$[\mathcal{H}, A] \,|\, 0 \rangle \equiv \left[\mathcal{H}, \sum_n \left(\alpha_n \tau_{2n}^- + \beta_n \tau_{2n+1}^- \right) \right] |\, 0 \rangle = E A \,|\, 0 \rangle . \tag{27}$$

Either calculation can be equally easily carried out with the original (non-sublattice-mapped) Hamiltonian.

3. *Dimers: Particle representation*

We now interpret the sublattice-mapped Hamiltonian (18) in terms of a mapped particle-vacancy picture ($\tau^z = \pm 1$ for particles or vacancies, respectively). For arbitrary site occupations and rates (ϵ, ϵ'), in this particle representation the deposition-evaporation process can be viewed as providing currents between the two sublattices such that

$$\frac{\partial \tilde{\rho}_l}{\partial t} = J_{l-1,l} - J_{l,l+1} , \tag{28}$$

where $J_{i,j}$ is the current from site i to the neighboring site j (see Fig. 3). These currents are completely determined because of the known exact steady states:

$$\begin{aligned} J_{2l,2l+1} &= \epsilon \tilde{\rho}_{2l} \left(1 - \tilde{\rho}_{2l+1} \right) - \epsilon' \tilde{\rho}_{2l+1} \left(1 - \tilde{\rho}_{2l} \right) , \\ J_{2l-1,2l} &= \epsilon' \tilde{\rho}_{2l-1} \left(1 - \tilde{\rho}_{2l} \right) - \epsilon \tilde{\rho}_{2l} \left(1 - \tilde{\rho}_{2l-1} \right) . \end{aligned} \tag{29}$$

Equations (28) and (29) constitute a mean field version of an exact equation for $d\langle \tau_l^z \rangle / dt$, and become exact for small deviations from the steady states [as in the discussion below, starting from Eq. (30)].

For $\epsilon = \epsilon'$ the sublattice distinction in the particle representation becomes irrelevant and the set of equations becomes a discrete linear diffusion equation. This can be used to derive the results already given in Sec. III B above.

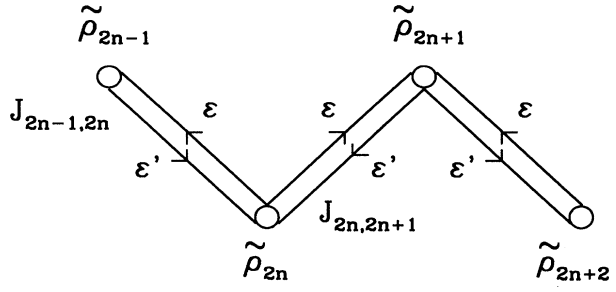

FIG. 3. Schematic description of particle currents in the sublattice-mapped representation [Eq. (29) in the text].

For $\epsilon \neq \epsilon'$ it is straightforward to consider deviations from steady states which are uniform on each sublattice

$$\begin{aligned} \tilde{\rho}_{2l+1} &= \tilde{\rho}_A + \delta_{2l+1}(t) \\ &= \tilde{\rho}_A + A \exp \left[iq(2l+1) - Et \right] , \\ \tilde{\rho}_{2l} &= \tilde{\rho}_B + \delta_{2l}(t) = \tilde{\rho}_B + B \exp \left[iq2l - Et \right] . \end{aligned} \tag{30}$$

Inserting into Eqs. (28) and (29) and eliminating B/A yields $(E-\alpha)(E-\beta) = \alpha\beta \cos^2 q$ with

$$\begin{aligned} \alpha &\equiv 2 \left[\epsilon - \tilde{\rho}_A (\epsilon - \epsilon') \right] , \\ \beta &\equiv 2 \left[\epsilon' + \tilde{\rho}_B (\epsilon - \epsilon') \right] , \\ \alpha\beta &= 4 \epsilon \epsilon' . \end{aligned} \tag{31}$$

For small q, it follows that $E \to D q^2$ where

$$D = \frac{\alpha\beta}{\alpha + \beta} = \frac{2\sqrt{\epsilon \epsilon' R_A R_B}}{R_A + R_B} , \tag{32}$$

where $R_\alpha \equiv \tilde{\rho}_\alpha (1 - \tilde{\rho}_\alpha)$. This provides the diffusive behavior and associated diffusion constant for arbitrary $\tilde{\rho}_A$, $\tilde{\rho}_B$, ϵ, ϵ' satisfying (31). For the special case $(\tilde{\rho}_A, \tilde{\rho}_B) \to (1,1)$ the result is that already derived in Sec. III B 2. We will make use of Eq. (32) to test the reliability of finite-size scaling methods to be introduced in Sec. VI, by measuring the diffusion velocity D for various $\tilde{\rho}_A$, $\tilde{\rho}_B$, ϵ, ϵ'.

An alternative method of deriving the diffusion constant is by a linear response method. Here a small field $\mathcal{E}$ is applied to induce a particle current $\mathcal{J}$

$$\begin{aligned} \mathcal{J} &= \epsilon \lambda \tilde{\rho}_A (1 - \tilde{\rho}_B) - \frac{\epsilon'}{\lambda} \tilde{\rho}_B (1 - \tilde{\rho}_A) , \\ \lambda &= \exp (\beta \mathcal{E}/2) , \\ &\to \sigma \mathcal{E} \equiv \beta \epsilon \tilde{\rho}_A (1 - \tilde{\rho}_B) \mathcal{E} , \quad \mathcal{E} \to 0 . \end{aligned} \tag{33}$$

We may then use the Einstein relation $D = \sigma/\chi$, where χ is the compressibility

$$\chi = \frac{\beta}{L} \sum_{i,j} \left(\langle n_i n_j \rangle - \langle n_i \rangle \langle n_j \rangle \right) = \frac{\beta}{2} \left(R_A + R_B \right) . \tag{34}$$

The result (32) again follows.

4. Flory limit

The process of dimer deposition introduced by Flory [2] is the prototype model for random sequential adsorption (RSA). It is thus interesting to see how Flory's results appear in our generalized model in the limit that the evaporation rate ϵ' approaches zero.

The Flory model exhibits a very large number of jammed steady states, none of which have two or more contiguous vacant sites; as $t \to \infty$, the system gets stuck in one of these jammed configurations. If the initial state is an empty lattice, the mean coverage has a saturation value $\Theta_F = (1 - e^{-2})$. This asymptotic result is very different from the value $\Theta_0 = 1$ obtained on taking the limit $\epsilon' \to 0$ in Eq. (21). Evidently, the limits $\epsilon' \to 0$ and $t \to 0$ do not commute.

The reason for this is not hard to see. A nonzero but small value of the evaporation rate ϵ' is associated with a large crossover time $t^* \sim 1/\epsilon'$. For $t \ll t^*$, there is a very small probability of an evaporation attempt at any given site, and the kinetics is dominated by deposition. Thus, Flory-like jammed states are approached exponentially in time [14] with rate ϵ for $1/\epsilon \ll t \ll t^*$.

On the other hand, over much longer time scales, $t \gg t^*$, the state of the system is quite different: it approaches the steady state described by Eq. (19). Correspondingly, the coverage approaches a value close to unity, as in Eq. (21). It is only on these time scales that the diffusion constant D of Eq. (32) describes the dynamical behavior.

5. Effect of single-particle diffusion

A striking effect occurs if the model is generalized to include explicit particle diffusion on the lattice, through a nearest-neighbor particle hopping term. This adds to the Heisenberg Hamiltonian (9) additional pair terms involving $\sigma_l^+ \sigma_{l'}^-$.

In terms of the sublattice-mapped τ-spin representation, the result is to add terms which break rotational invariance in the XY plane. In the case of equal deposition and evaporation rates $\epsilon = \epsilon'$ and equal forward and backward hopping rate h, the corresponding evolution operator results in the XYZ Hamiltonian

$$\mathcal{H} = -\frac{1}{2} \sum_l \left[(\epsilon + h)\, \tau_l^x \tau_{l+1}^x + (\epsilon - h)\, \tau_l^y \tau_{l+1}^y + (\epsilon - h)\, \tau_l^z \tau_{l+1}^z - (\epsilon + h) \right] . \quad (35)$$

As a result, a gap Δ develops in the spin-wave spectrum and the autocorrelation function becomes proportional to $\exp(-\Delta t)$ at long times. In addition, the lack of isotropy in the XY plane removes the hidden continuous symmetry to be referred to in Sec. V. So, explicit particle diffusion instead of augmenting the diffusive power-law tail converts it to exponential decay. This behavior is again confirmed by Monte Carlo simulations [Fig. 2(a)].

IV. $k \geq 3$: BROKEN ERGODICITY, PARTIAL JAMMING, AND DIFFUSIVE DECAY

A. Number of subspaces

The case of trimers is typical of k-mers for $k \geq 3$ and differs from the dimer case in a basic respect: the full phase space of 2^L Ising (site occupation) configurations splits into a very large number $I(k, L)$ of invariant subspaces which are not connected to each other by the dynamics induced by the stochastic operator. For $k \geq 3$, the number $I(k, L)$ grows exponentially with L (see Fig. 4) in contrast to $I(2, L)$ which increases as $L+1$ for even L.

The exponential growth can be established as follows. Let $I_1(k, L)$ be the number of invariant subspaces of size 1 and write $I(k, L) = I_1(k, L) + I^*(k, L)$. Here $I^*(k, L)$ is the number of subspaces with nontrivial dynamics, each of which has more than one configuration in it. We may estimate $I_1(k, L)$ on noting that each subspace of size 1 corresponds to a completely jammed configuration, one which is left invariant by the stochastic evolution operator. Each such configuration is characterized by having no more than $k - 1$ successive parallel spins anywhere along the lattice. The number $I_1(k, L)$ of configurations may be calculated using a recurrence method, sketched in Appendix C. For an open chain of length L, the answer is

$$I_1(k, L) = 2\, F_k(L) , \quad (36)$$

where $F_k(L)$ is a generalized Fibonacci number defined

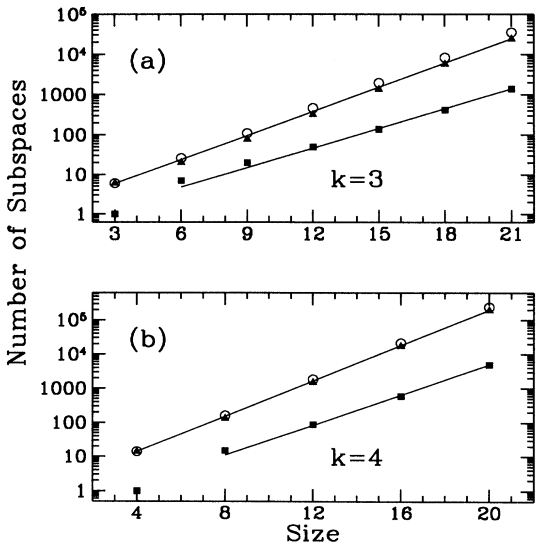

FIG. 4. Number of subspaces of the evolution operator vs system size for (a) $k = 3$ and (b) $k = 4$. The squares and triangles denote partially and fully jammed number of subspaces, respectively, for periodic boundary conditions. Both indicate an exponential growth. The circles are the analytic determination of fully jammed subspaces for open boundary conditions. Solid lines are guides to the eye.

by the recursion (C9)–(C11) in Appendix C. The asymptotic result is

$$I_1(k,L) \sim \lambda^L , \tag{37}$$

where λ is the largest root of $\lambda^k = 2\lambda^{k-1} - 1$. For $k = 3$, λ is the golden mean $\simeq 1.618$, while for $k = 4$, $\lambda \simeq 1.839$. As we see from Fig. 4, the total number of subspaces $I(k,L)$ too grows as λ^L.

The stochastic operator has a nontrivial action in each of the $I^*(k,L)$ dynamically nontrivial invariant subspaces. We have investigated the splitting of H into disconnected sub-blocks in the Ising or particle representation on rings of sizes $3 \leq L \leq 21$. The idea of the underlying exact enumeration algorithm can be implemented easily. We choose an arbitrary initial state from the 2^L possible configurations and apply H to it keeping proper track of the newly generated configurations (if any) until exhausting the subspace to which this state belongs. Repeating this operation with successive new states that are not already included in the previously generated subspaces, we obtain finally a complete classification of configurations according to their corresponding sub-blocks. The number of total invariant subspaces and the particular configurations contained on them is of course independent of ϵ and ϵ' provided that both rates have nonzero values.

It turns out that $I^*(k,L)$ too grows exponentially with L (see Fig. 4). Writing $I^*(k,L) \sim \mu^L$ and using periodic chains with L a multiple of k to avoid spurious finite-size effects, we find that successive ratios $I^*(k,L+k)/I^*(k,L)$ increase with L, making a reliable numerical estimate of μ difficult. However, extrapolations involving finite-size correction terms are helpful at least to determine lower bounds. Our data suggest $\mu > 1.4$ for $k = 3$ and $\mu > 1.6$ for $k = 4$. Recent work [15] employing free-boundary conditions shows that it is possible to set up and solve recursions for $I^*(k,L)$, and thus deduce $\mu = \lambda$.

The behavior of $I_1(k,L)$ and $I^*(k,L)$ implies that the full space is divided into an exponentially large number of subspaces, each of which is dynamically decoupled from the others. Our model is thus strongly nonergodic, making it quite unusual. Further, since each invariant subspace typically contains very many configurations, almost all of the full set of configurations belong to the $I^*(k,L)$ partially jammed subspaces. (The remainder, the jammed configurations, constitute a fraction $\sim (\lambda/2)^L$, which vanish rapidly as $L \to \infty$.)

Let us take the initial state to be a single specified configuration $|\{\sigma_l^z\}\rangle$ in the Ising basis. It belongs to a particular invariant subspace, call it Λ. The time evolution within this subspace is governed by H_Λ, i.e., the sub-block of H corresponding to that subspace. Since H_Λ is a stochastic matrix, it follows from the conservation of probability that H_Λ $(1,1,\ldots,1)$ is a left eigenvector of H_Λ with eigenvalue 0. The corresponding right eigenvector specifies the unique steady state, which we denote by $|\Lambda,0\rangle$. In the case $\epsilon = \epsilon'$ the stochastic matrix H_Λ is symmetric and the steady state (right eigenvector) is $(1,1,\ldots,1)$ as well. Every microscopic configuration is weighted equally in the steady state. It is possible to write down the steady state in the case $\epsilon \neq \epsilon'$ as well, noting that detailed balance implies that configurations C and C' both in Λ, which differ from each other only by a single deposition, have relative weights in the ratio ϵ/ϵ'.

Since each invariant subspace Λ has a unique steady state $|\Lambda,0\rangle$ the total degeneracy of steady states of H is $I(k,L)$. Hence it is possible to form other steady states from linear combinations over $|\Lambda,0\rangle$. For instance, steady states described at the beginning of Sec. V B are of this type.

B. Jamming

We have seen that the steady states $|\Lambda,0\rangle$ are either completely jammed configurations or a linear combination of evolving configurations. Even a steady state of the latter sort is partially jammed in a sense that can be made quantitative, as discussed below.

The dynamics in steady state involves a succession of stochastic transitions between states $|s\rangle = |\{\sigma_l^z\}\rangle$ in Λ. The mean rate per site of such transitions is

$$\begin{aligned} J(\Lambda) &= \frac{1}{L}\left\langle \Lambda,0 \left| \sum_n R_n \right| \Lambda,0 \right\rangle \\ &= \frac{1}{L}\sum_{s\in\Lambda}\sum_{s'\neq s} P_0(s)\, W(s \to s') , \end{aligned} \tag{38}$$

where $P_0(s)$ are the equilibrium probabilities. Hence $J(\Lambda)$ is a quantitative measure of the lack of jamming in that steady state. For instance, for completely jammed steady states, $J = 0$. The steady state $|\Lambda_E,0\rangle$ resulting from an all-empty initial configuration has the least jamming of all.

Using the exact enumeration algorithm described above we can characterize the exact steady state in all subspaces for $\epsilon = \epsilon'$ since the rows of H add up to zero and therefore $P_0(s) \equiv 1/N_\Lambda$, where N_Λ is the total number of configurations in the Λ subspace.

We computed $J(\Lambda)$ in various subspaces on finite systems with $3 \leq L \leq 21$. The corresponding "currents" are largest in the E subspace, which includes the all-empty configuration. The result is $J_E \simeq 0.35$ for $k = 3$ and $J_E \simeq 0.29$ for $k = 4$, both indicating a fairly large degree of jamming.

Monte Carlo simulations again confirm a diffusive decay of autocorrelation functions in this particular translationally invariant subspace, both for equal and different deposition-evaporation rates, as is shown in Figs. 2(a) and 2(b), respectively. Moreover, the broken ergodicity and the lack of translational invariance of most subspaces does not affect the diffusive behavior observed so far. The results obtained in the trimer case on one such subspace can be seen in Fig. 5. Here the starting configuration is a Néel state with every sixth spin reversed.

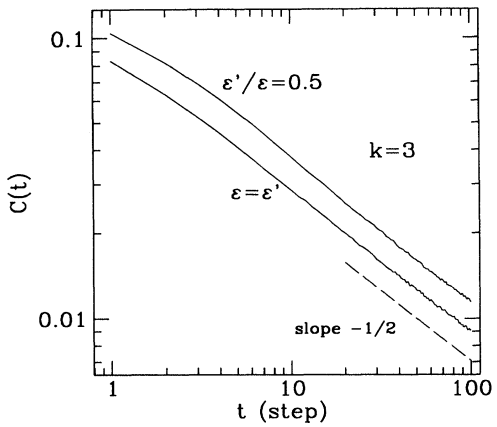

FIG. 5. Autocorrelation function for deposition and evaporation of trimers in the steady state reached from an initial Néel configuration with every sixth spin reversed. The averages were taken over 100 samples for $L = 1.2 \times 10^5$ and $\epsilon'/\epsilon = 0.5$, 1 both indicating a power-law decay ($\sim t^{-1/2}$).

C. Diffusive decays in nearly jammed configurations

The diffusive decay seen in the trimer system can be discussed for the case of almost jammed states by random-walk arguments, like those in Sec. III B for the dimer system.

The first example considered is the random walk of simple spin flips on the jammed periodic state $|\psi\rangle = (\uparrow\uparrow\downarrow)^{L/3} \equiv \uparrow\uparrow\downarrow\uparrow\uparrow\downarrow \ldots$. The state $|\psi_l\rangle = \sigma_{3l}^{+}|\psi\rangle$ involves a cluster of five up spins on which the trimer Hamiltonian H can act. It is found that $(H + 3\epsilon)|\psi_l\rangle$ produces three new states

$$\begin{aligned} |\psi_l^1\rangle &= \sigma_{3l-2}^{-}\sigma_{3l-1}^{-}|\psi\rangle, \\ |\psi_l^2\rangle &= \sigma_{3l-1}^{-}\sigma_{3l+1}^{-}|\psi\rangle, \\ |\psi_l^3\rangle &= \sigma_{3l+1}^{-}\sigma_{3l+2}^{-}|\psi\rangle. \end{aligned} \tag{39}$$

$|\psi^1\rangle$ and $|\psi^3\rangle$ involve a cluster of four down spins, and $|\psi^2\rangle$ a cluster of three down spins. The trimer Hamiltonian H again has nontrivial action on these states, namely,

$$\begin{aligned} (H + 3\epsilon')|\psi_l\rangle &= \epsilon'\left(|\psi_l^1\rangle + |\psi_l^2\rangle + |\psi_l^3\rangle\right), \\ (H + 2\epsilon)|\psi_l^1\rangle &= \epsilon\left(|\psi_{l-1}\rangle + |\psi_l\rangle\right), \\ (H + \epsilon)|\psi_l^2\rangle &= \epsilon|\psi_l\rangle, \\ (H + 2\epsilon)|\psi_l^3\rangle &= \epsilon\left(|\psi_l\rangle + |\psi_{l+1}\rangle\right). \end{aligned} \tag{40}$$

After eliminating the new states we have

$$\begin{aligned} &[(H+\epsilon)(H+2\epsilon)(H+3\epsilon') - \epsilon\epsilon'(3H+4\epsilon)]\,|\psi_l\rangle \\ &\quad = \epsilon\epsilon'(H+\epsilon)\left(|\psi_{l-1}\rangle + |\psi_{l+1}\rangle\right). \end{aligned} \tag{41}$$

This equation describes a generalized random walk of the original spin flip state. Eigensolutions of the form $\propto \exp(iql)$ yield the secular equation for the eigenenergy E

$$\begin{aligned} &E^3 + 3E^2(\epsilon+\epsilon') + E\left[2\epsilon^2 + 2\epsilon\epsilon'(3-\cos q)\right] \\ &\quad + 2\epsilon^2\epsilon'(1-\cos q) = 0. \end{aligned} \tag{42}$$

Of the three resulting branches, the lowest is gapless having $E(q)$ going to zero as $q \to 0$ like $E \sim Dq^2$ with (diffusion) constant D

$$D = \frac{\epsilon\epsilon'}{4\epsilon' + 2\epsilon}. \tag{43}$$

Taking into account Eq. (39) and considering the secular equation $[H, A_q]\,|\psi\rangle = E(q)\,A_q\,|\psi\rangle$ it is straightforward to show that the eigenstate is $A_q|\psi\rangle$ where

$$\begin{aligned} A_q = \sum_l \exp(iql)\Bigg[\sigma_{3l}^{+} + \frac{\epsilon'}{2\epsilon + E(q)}\cos\frac{q}{2}\big[\exp(-iq/2)\,\sigma_{3l-2}^{-}\sigma_{3l-1}^{-} \\ + \exp(iq/2)\,\sigma_{3l+1}^{-}\sigma_{3l+2}^{-}\big] + \frac{\epsilon'}{\epsilon + E(q)}\sigma_{3l-1}^{-}\sigma_{3l+1}^{-}\Bigg]. \end{aligned} \tag{44}$$

The form of this creation operator is consistent with more general considerations to be given in Sec. V. Also $[A_0, H]\,|\psi\rangle = 0$, so A_0 creates a new steady state from the fully jammed state $|\psi\rangle$.

A second example is the random walk of spin flips on the fully jammed antiferromagnetic periodic state $|\varphi\rangle = (\uparrow\downarrow)^{L/2} = \uparrow\downarrow\uparrow\downarrow \ldots$. In Appendix D it is shown that repeated application of the Hamiltonian H to the initial state $\sigma_l^{-}|\varphi\rangle$ generates a random walk of a group of three up or three down spins on the antiferromagnetic background. The equation yielding the eigenenergies is shown to be

$$E_q^2 - 2E_q(\epsilon+\epsilon') + 4\epsilon\epsilon'\sin^2 q = 0. \tag{45}$$

The gapless "acoustic" branch yields diffusive behavior $E \to Dq^2$ for small q with

$$D = \frac{2\epsilon\epsilon'}{\epsilon + \epsilon'}. \tag{46}$$

There is a remarkable similarity of both D and E_q to the quantities occurring for the dimer case $k = 2$, $\epsilon \neq \epsilon'$ with the same antiferromagnetic fully jammed state.

Walks of several defects on more general fully jammed states can be considered in a similar way. For instance, Fig. 6(a) displays a particular evolution of five walkers embedded in a jammed antiferromagnetic background showing that the concept of "walker" is well defined in this case. Figure 6(b) shows schematically the corresponding trimer random walk on a microprocess level where again the walker is well defined. However, it is instructive to verify that this is not always the case as can be seen in Fig. 6(c) which displays a particular history of an initial random configuration containing at most three nearest-neighbor parallel spins. Here the "single" active patch may eventually split into many other walkers. Additionally, it may not be correct to assume that even in a finite walker density regime, collisions and interactions among walkers have no important consequences at long times, other than to modify the actual value of the diffusion constant.

Also, a simple particle description like that in Sec. III B 3 for the dimer case does not seem possible for $k = 3$. However, symmetry properties of the k-mer Hamiltonian, which will be discussed in Sec. V, provide a partial explanation of the diffusive behavior seen generally for trimers.

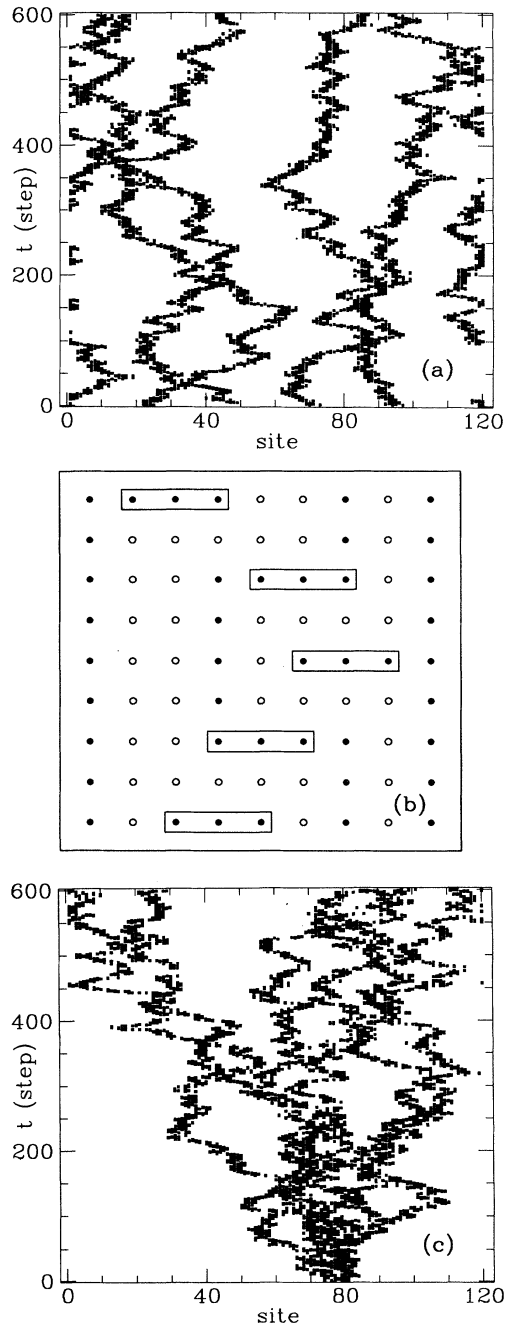

FIG. 6. (a) A particular trimer evolution of unjammed regions through an antiferromagnetic jammed background, displaying a random-walk behavior; only updated spins are shown. (b) A schematic view of active trimers (denoted by rectangles) evolving through deposition-evaporation processes in an antiferromagnetic background. (c) A particular trimer history starting from a fully jammed random state containing at most three parallel spins, exhibiting a split into many walkers.

V. CONSERVED QUANTITIES, SYMMETRIES, AND GOLDSTONE BOSONS

It is well known that conserved quantities, continuous symmetries, and slow kinetics are closely interelated. The long wavelength fluctuations of a macroscopic conserved quantity show hydrodynamic or diffusive dynamic behavior; this can cross over to critical behavior if the velocity or diffusion constant vanishes.

A continuous symmetry implies a conserved quantity since the generator of the symmetry commutes with the Hamiltonian. When a ground state breaks such a continuous symmetry, a gapless band of Goldstone bosons is implied.

These concepts can be used to provide an understanding of the slow asymptotic kinetics seen in the deposition-evaporation models. The diffusive decay seen for dimers with equal rates ($\epsilon = \epsilon'$) has already been interpreted in terms of spin waves (Sec. III): these are the Goldstone bosons implied by the full rotation symmetry of the isotropic Heisenberg Hamiltonian (19). Furthermore, the conserved quantities can help to categorize the invariant subspaces described in Sec. VI.

These ideas are developed in Secs. V A–V C, which treat in turn, conserved quantities, symmetries, and Goldstone bosons.

A. Conserved quantities

For the case of monomers ($k = 1$) the Hamiltonian (15) is a sum of single-spin terms, so each of these is a constant of motion. These constants completely describe the breakup into invariant subspaces but they are not macroscopic quantities, so no slow dynamics is implied

and of course the decay is exponential in time.

For dimers with $\epsilon = \epsilon'$, each component of $\mathbf{T} \equiv \sum_l \boldsymbol{\tau}_l$ is a constant of motion. These components generate arbitrary rotations of all spins along the corresponding axes, and the conservation law is related to the full rotation symmetry of the Hamiltonian. The spin-wave Goldstone modes and the resulting diffusive decay follow from the breaking of this symmetry by the parallel-spin ground states.

The situation is more complicated for $\epsilon \neq \epsilon'$ or for $k > 2$. However, it can be shown that for arbitrary k and ϵ'/ϵ the most general local constant of motion involving only spin z components is of the form

$$Q = \sum_l C_l \sigma_l^z \tag{47}$$

(excluding a trivial additive constant).

Further, by considering $[H, Q] = 0$, it can be shown that

$$\sum_{n=l}^{l+k-1} C_n \equiv 0 \quad \forall\, l\,. \tag{48}$$

This linear equation is easy to solve and results in Q being an arbitrary linear combination of $Q_1, Q_2, \ldots, Q_{k-1}$ where

$$Q_r = \sum_l \lambda_r^l \sigma_l^z, \quad \lambda_r \equiv \exp(i2\pi r/k)\,. \tag{49}$$

where $r = 1, 2, \ldots, k-1$ so that λ_r runs over the nontrivial roots of unity. Equivalently, Q can be written as an arbitrary linear combination of the $k-1$ independent conserved quantities already identified in Sec. II, i.e., $M_\alpha - M_k$, $\alpha = 1, 2, \ldots, k-1$, where M_α is the z component of the total spin on sublattice α. For the case $k = 2$, $\epsilon = \epsilon'$ the resulting single conserved quantity is $T^z \equiv \sum_l \tau_l^z$ and this is related to the symmetry of the isotropic Heisenberg Hamiltonian (19) with respect to rotations around the z axis. It will be shown in Secs. V B and V C that the conserved quantities $M_\alpha - M_k$ arise from a continuous symmetry of the Hamiltonian for general k, ϵ'/ϵ and that this gives a partial understanding of the slow kinetics seen in general.

The conserved quantities discussed above appear to be the only ones involving *local* combinations of spin operators for $k \geq 3$. They are, for any k, the only ones diagonal in the Ising basis. An initial state which is a single specified configuration in the Ising basis is labeled by particular values of each of these conserved quantities which do not change under the time evolution produced by the Hamiltonian.

B. Symmetries

Under a rotation by an angle φ_l around the spin z axis, the transverse components of spin $\boldsymbol{\sigma}_l$ transform according to

$$\begin{aligned} \sigma_l^x &\to \sigma_l^x \cos\varphi_l - \sigma_l^y \sin\varphi_l\,, \\ \sigma_l^y &\to \sigma_l^x \sin\varphi_l + \sigma_l^y \cos\varphi_l\,. \end{aligned} \tag{50}$$

Equivalently

$$\sigma_l^\pm \to \sigma_l^\pm \exp(\pm i\varphi_l)\,. \tag{51}$$

Such a rotation leaves $\prod \sigma_l^+$, $\prod \sigma_l^-$ and all other terms in the Hamiltonian (9) unchanged provided that

$$\sum_{r=1}^{k} \varphi_{l+r} = 0 \quad \forall\, l\,. \tag{52}$$

This condition requires a common rotation angle $\varphi_l = \varphi_\alpha$, for all spins l on sublattice α with the constraint

$$\sum_{\alpha=1}^{k} \varphi_\alpha = 0\,. \tag{53}$$

This condition permits $k-1$ independent arbitrary rotation angles. So for $k \geq 2$ the Hamiltonian is invariant under the continuous z-rotation symmetry expressed by the above equations. For $k = 2$ the sublattice-mapped version of condition (53) is the common z rotation of all spins.

We next show how the $k-1$ conserved quantities identified in Sec. V A result from this continuous symmetry.

The rotations described above are generated by the operator

$$Q \equiv \sum_{\alpha=1}^{k} \varphi_\alpha M_\alpha^z\,, \tag{54}$$

where $M_\alpha^z \equiv \sum_l \sigma_{kl+\alpha}^z$ and the angles φ_α satisfy Eq. (53).

The invariance of $H = \exp(iQ/2)\, H \exp(-iQ/2)$ implies $[H, Q] = 0$. Q is therefore a conserved quantity. Furthermore, it involves $k-1$ independent conserved quantities since $k-1$ of the angles are independent, hence

$$\begin{aligned} Q &= \sum_{\alpha=1}^{k-1} \varphi_\alpha M_\alpha^z + M_k^z \left(-\sum_{\alpha}^{k-1} \varphi_\alpha \right) \\ &= \sum_{\alpha=1}^{k-1} \varphi_\alpha (M_\alpha^z - M_k^z)\,. \end{aligned} \tag{55}$$

The $k-1$ angles involved in the last sum are now independent. We thus recover the $k-1$ conserved quantities $M_\alpha^z - M_k^z$ as a consequence of the continuous symmetry. In the next subsection we will discuss how broken symmetries, Goldstone bosons, and slow kinetics arise from this continuous symmetry.

It should be noted that the above account of symmetries is not complete. For example, the full rotation symmetry of the sublattice-mapped Hamiltonian (19) for the case $k = 2$, $\epsilon = \epsilon'$ arises from the continuous symmetry discussed above together with an additional property, namely, conservation of probability – this latter property

is reflected in the vanishing of each column sum in the matrix representation of H.

C. Broken symmetries, Goldstone bosons, and slow kinetics

The continuous z-rotation symmetry introduced above in Sec. V B is not broken by the fully jammed steady states, since they are eigenstates of each σ_l^z.

A class of steady states which break the symmetry can be constructed from the form of the alternative form of the Hamiltonian given in Sec. II, Eq. (11). These steady states are product eigenstates of ξ_l with eigenvalues $m_l = \pm 1$ such that $m_l = m_\alpha$ for l on sublattice α with $\prod_{\alpha=1}^{k} m_\alpha = 1$.

These states are linear combinations of all the steady states $|\Lambda, 0\rangle$ already introduced in Sec. IV. Applying the z-rotation symmetry (51)–(53) to them produces new steady states. Since they break this continuous symmetry the existence of Goldstone bosons is implied. We now develop these ideas in a little more detail.

If $|0\rangle$ denotes the state with all spins up, the steady states formed from product eigenstates of $\xi_l \equiv \gamma\sigma_l^+ + \gamma^{-1}\sigma_l^-$, $\gamma = (\epsilon/\epsilon')^{1/k}$ are

$$|\xi\rangle = \frac{\gamma^L}{(\gamma^2+1)^{L/2}} \prod_l \left(1 + \frac{m_l}{\gamma}\sigma_l^-\right)|0\rangle . \tag{56}$$

Applying the z-rotation generator Q of Eq. (47) to these states produces the new steady states (omitting the normalization prefactor)

$$\exp\left(i\frac{Q}{2}\right)|\xi\rangle = \prod_l \left[\exp(i\varphi_l/2) + \frac{m_l}{\gamma}\exp(-i\varphi_l/2)\,\sigma_l^-\right]|0\rangle , \tag{57}$$

where m_l and φ_l satisfy the conditions given above and in (53).

Still more general steady states can be produced by exploiting the $k-1$ independent angles among the $\{\varphi_\alpha\}$. The most general steady state is the linear combination with an arbitrary weight function f, namely,

$$|\psi_{\{f\}}\rangle = \int\cdots\int \left(\prod_{\alpha=1}^{k-1} d\varphi_\alpha\right) f(\varphi_1, \ldots, \varphi_{k-1}) \prod_{l=1}^{L/k} \left[\prod_{\alpha=1}^{k-1} \left(\exp(i\varphi_\alpha/2) + \frac{m_\alpha}{\gamma}\exp(-i\varphi_\alpha/2)\,\sigma_{kl+\alpha}^-\right) \times \left(\exp(i\Theta/2) + \frac{m_k}{\gamma}\exp(-i\Theta/2)\,\sigma_{k(l+1)}^-\right)\right]|0\rangle , \tag{58}$$

$$\Theta \equiv -\sum_{\alpha=1}^{k-1}\varphi_\alpha .$$

This form is appropriate for a chain of L sites with L an integer multiple of k.

If the arbitrary weighting function is chosen to pick out arbitrary powers p_α of $x_\alpha \equiv \exp(-i\varphi_\alpha)$, $\alpha = 1, \ldots k-1$, a steady state with a definite difference p_α of occupations of αth and kth sublattices can be produced. It is the coefficient of $\prod_{\alpha=1}^{k-1} x_\alpha^{p_\alpha}$ in $\exp(\mathcal{A}\{x_\alpha\})\,|(\uparrow\uparrow\cdots\downarrow)^{L/k}\rangle$, where

$$\begin{aligned} \mathcal{A} &\equiv \sum_{\alpha=1}^{k-1} x_\alpha \mathcal{J}_\alpha^- + \left(\prod_{l=1}^{k-1} x_l\right)\mathcal{J}_k^+ \quad , \\ \mathcal{J}_\alpha^\pm &\equiv m_\alpha \alpha^{\pm 1}\mathcal{S}_\alpha^\pm , \\ \mathcal{S}_\alpha^\pm &\equiv \sum_l \sigma_{kl+\alpha}^\pm , \end{aligned} \tag{59}$$

and $|(\uparrow\uparrow\cdots\downarrow)^{L/k}\rangle$ is the state with every kth spin down in a set of up spins. For $k \geq 2$ the total number of steady states produced by this procedure is of order L^{k-1}, of which only $2k$ are fully jammed. Clearly this constitutes a vanishingly small fraction of all the $I(k, L)$ steady states (see Sec. IV).

In the expansion

$$\exp\mathcal{A} \equiv \sum_{p_1}\cdots\sum_{p_{k-1}} \left(\prod_{\alpha=1}^{k-1} x_\alpha^{p_\alpha}\right)\hat{\Theta}^{(p_1,\ldots,p_{k-1})} , \tag{60}$$

the operators $\hat{\Theta}^{(p_1,\ldots,p_{k-1})}$ generate from $|(\uparrow\uparrow\cdots\downarrow)^{L/k}\rangle$ the steady states described above. They can also be shown to act as raising operators for the conserved quantities Q_r given in Sec. V A. Since they derive from a continuous symmetry of the Hamiltonian, q-dependent generalizations of them create the Goldstone bosons. For example, for $k = 3$, q-dependent generalizations of $\hat{\Theta}^{(1,0)} = (m_1/\alpha)\mathcal{S}_1^-$ and $\hat{\Theta}^{(0,1)} = (m_2/\alpha)\mathcal{S}_2^-$ do not produce Goldstone bosons since $H\sigma_{3l+\alpha}^-|(\uparrow\uparrow\downarrow)^{L/3}\rangle = 0$, $\alpha = 1, 2$. The first nontrivial

case is obtained from $\hat{\Theta}^{(1,1)} = (m_3/\alpha^2)(\mathcal{S}_1^- \mathcal{S}_2^- + \alpha^3 \mathcal{S}_3^+)$ using the property $m_1 m_2 m_3 = 1$. The q-dependent generalization creating the Goldstone bosons is the related form given in Eq. (44), Sec. IV.

The property $H \hat{\Theta}^{(p_1,\cdots,p_{k-1})} |(\uparrow\uparrow \ \ldots \ \downarrow)^{L/k}\rangle = 0$ (e.g., with $k = 3$, $p_1 = p_2 = 1$ for the particular case just being illustrated) is enough to ensure the gapless character of the spectrum as $q \to 0$, and the resulting diffusive power-law decay of the autocorrelation function.

VI. FINITE-SIZE SCALING AND UNIVERSALITY

Although the Monte Carlo simulations of Secs. III and IV detected a diffusive decay in the autocorrelation functions for $k \geq 2$, they also indicate that our statistics become noisy beyond times of the order of 100 steps. Of course this situation could be improved simply by averaging over many more histories, although this alternative is prohibitive for our available computer time. We have tried to enlarge the number of samples at the expense of reducing the relaxation time t_0 but it turns out that correlation effects between histories become important. Integration or "smoothing" of numerical data may give misleading results in some cases.

However, since any *finite* system asymptotically has strictly an exponentially fast kinetics, the above difficulties can be surmounted using smaller systems and finite-size scaling arguments. On fairly general grounds, we expect the autocorrelation function $C(L,t)$ to be of scaling form

$$C(L,t) \equiv \frac{1}{L} \sum_l [\langle n_l(0)\, n_l(t)\rangle - \langle n_l\rangle^2] , \\ = \frac{t^{-\theta}}{b} Y(a\, t/L^z) , \tag{61}$$

where θ and z are critical exponents, and Y is a scaling function. θ, z, and Y are expected to be universal over all members of a given class, while a and b are nonuniversal metric functions. Hence we may assume that the relaxation time scales as L^z, thus finite-size scaling techniques allow in practice for both enlarging significantly the number of histories (time $\propto L$) and reducing the waiting time ($t_0 \propto L^z$). We explored sizes in the range $12 \leq L \leq 72$ waiting a time t_0, larger than the L-dependent relaxation time of the full lattice, to allow the system to reach steady state. The dynamical correlations were measured and averaged over 10^6 different histories.

We chose to explore three particular invariant subspaces, which were picked by specifying the initial configuration. The initial configurations were (i) all empty sites, (ii) the configurations obtained from the antiferromagnetic Néel state by reversing every sixth spin, (iii) half the system in an all-empty state; the other half in an antiferromagnetic state.

We now discuss the behavior in each of the subspaces (i), (ii), and (iii).

(i) This is the least jammed subspace of all subspaces. We studied the cases $k = 2, 3, 4$. On setting $z = 2$, $\theta = 1/2$, the data converge towards a universal curve for each value of k as it is shown in Figs. 7(a) and 7(b) for the cases $k = 3$ and $k = 4$, respectively. Moreover, by sliding the curves sideways and upward on the log-log scale [choosing the metric factors a and b in Eq. (61)], all the data are seen to collapse onto a single universal curve as can be observed in Fig. 8.

The scaling function can in fact be calculated analytically (solid curve in Fig. 8). This is because for $\epsilon = \epsilon'$ the dimer problem maps to the Heisenberg model, and can be solved on a finite ring. Following the calculation of Appendix B we find

$$C(L,t) = \frac{\tilde{\rho}\,(1-\tilde{\rho})}{L-1} \sum_{l\neq 0} \exp\left[-2\epsilon\left(1 - \cos\frac{2\pi l}{L}\right) t\right] . \tag{62}$$

The term with $l = 0$ is excluded as it corresponds to the uniform part, which is subtracted away in defining $C(L,t)$. In the scaling limit $L \to \infty$, $t \to \infty$ with $y \equiv \epsilon t/L^2$ held constant, we obtain

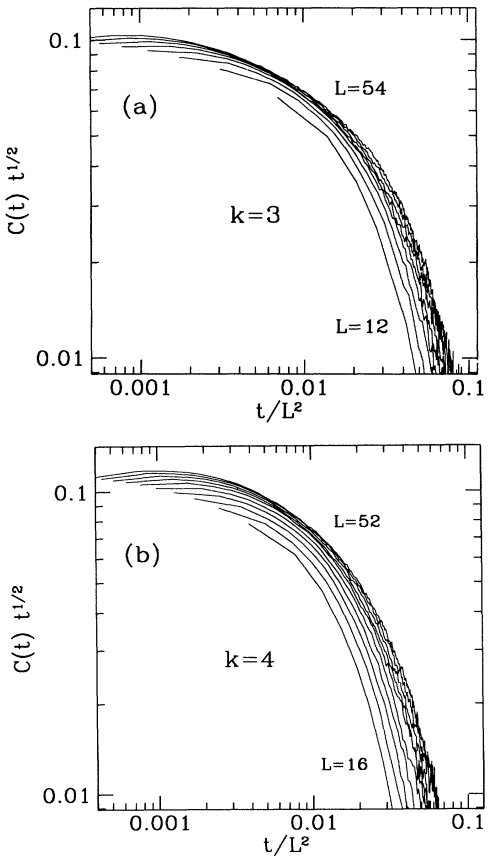

FIG. 7. Evidence for the finite-size scaling hypothesis for the autocorrelation function. The averages were taken over 10^6 histories for (a) $k = 3$ with sizes $L = 6m$, $2 \leq m \leq 9$ and for (b) $k = 4$ with $L = 4m$, $4 \leq m \leq 13$.

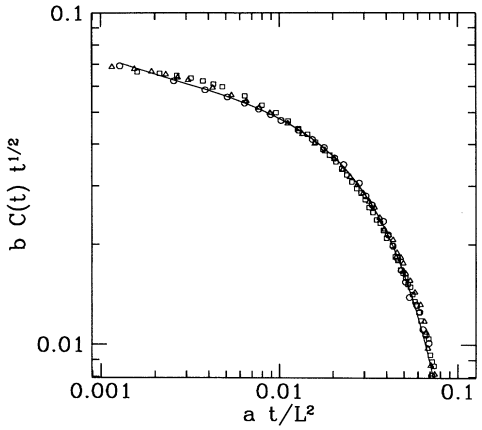

FIG. 8. Evidence for universality of k-mer kinetics from finite-size scaling, for steady states reached from an initially empty lattice. The data were averaged over 10^6 samples for $k = 2$, $L = 28$ (circles), $k = 3$, $L = 54$ (triangles), and $k = 4$, $L = 52$ (squares); a and b are metric factors referred to in the text. The solid line is the theoretical prediction for the scaling function [Eq. (63) in the text].

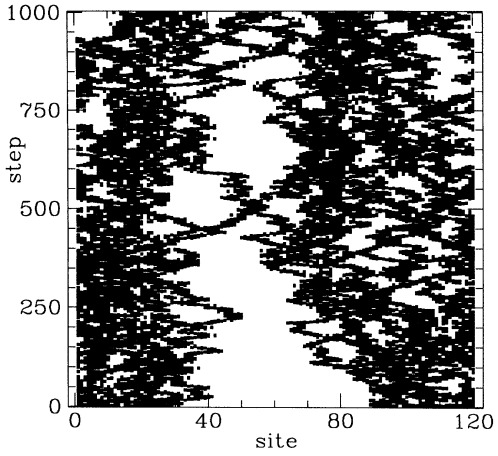

FIG. 9. Particular trimer evolution starting from a configuration in which half of the lattice is empty and the rest in an antiferromagnetic state (lower central white region), referred to as subspace (iii) in the text. Only updated spins are shown.

$$C(t) \simeq \tilde{\rho}\,(1-\tilde{\rho})\,(\epsilon t)^{-\frac{1}{2}}\,Y(y)\,,$$
$$Y(y) = y^{\frac{1}{2}} \sum_{l\neq 0} \exp\left(-4\pi^2 l^2 y\right)\,. \tag{63}$$

The sum that appears in the definition of the scaling function $Y(y)$ in Eq. (63) is related to the Jacobi theta function of the third kind [16].

(ii) This subspace differs from (i) in that the conserved quantity $(M_\alpha - M_\beta)$ is nonzero, implying that the average site occupation depends on the sublattice the site belongs to, i.e., the system is not translationally invariant.

Nevertheless, as with (i), good data collapse is found on choosing $z = 2$, $\theta = \frac{1}{2}$. Thus the dynamics is diffusive once again, confirming the results already obtained in large systems (Fig. 5).

(iii) Like (i), this subspace is translationally invariant. However, the dynamics seems to be quite different at least over the range of sizes studied. Figure 9 exhibits a particular evolution of the system starting from the initial state (iii) defined above. No collapse is found when $z = 2$, $\theta = \frac{1}{2}$ is used [Fig. 10(a)], while a rather good collapse is obtained by trying $z = \frac{1}{2}$, $\theta = \frac{1}{2}$ [Fig. 10(b)]. We used $t_0 = 400$ to generate the data shown in Figs. 10(a) and 10(b), but careful checks on several of the data points show that neither increasing t_0 to 3000 nor using different starting configurations makes a difference to the result. The scaling behavior in this subspace contrasts with the diffusive behavior in (i) and (ii). We do not have at present a clear understanding of this behavior. A possibility is that there are strong corrections to the diffusive scaling law in the range studied, and that the asymptotic scaling form (61) would set in for large enough sizes.

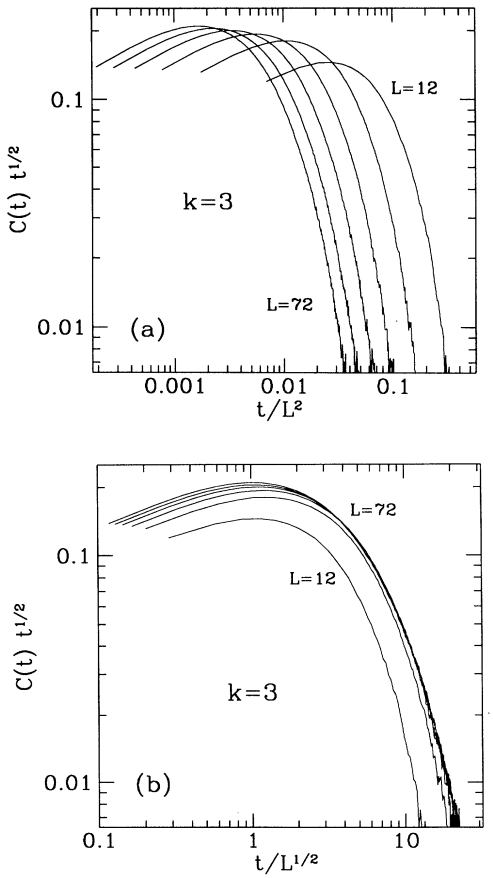

FIG. 10. The autocorrelation function averaged over 10^6 samples for $k = 3$ within subspace (iii) in the text. (a) Lack of data collapse on choosing a dynamic critical exponent $z = 2$. (b) Data collapse obtained with $z = 1/2$. Lattice widths are $L = 12m$, $1 \leq m \leq 6$.

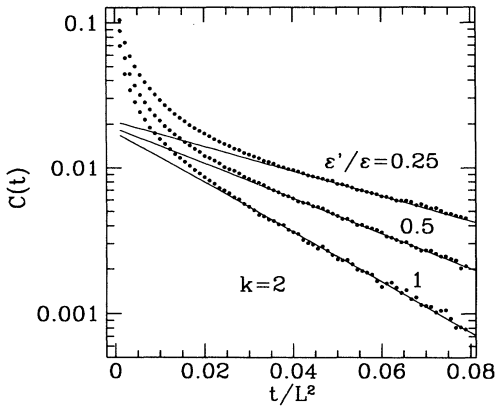

FIG. 11. Estimation of the diffusion constant D in the steady state for $k = 2$, $L = 30$ and $\epsilon'/\epsilon = 0.25, 0.5, 1$ starting from an all-empty lattice configuration and averaging over 10^6 histories. The solid lines are the asymptotic solutions of Eq. (63) in the text, their slopes being $4\pi^2 D \log_{10} e$.

Finally, the case of dimers offers again the possibility to test our Monte Carlo calculations now combined with the finite-size scaling hypothesis of Eq. (61). Simulations have been performed to measure diffusion constants for various ϵ, ϵ' and $\tilde{\rho}_A, \tilde{\rho}_B$ where $\tilde{\rho}_\alpha$ are the average occupation on the two sublattices $\alpha = A, B$. On identifying the metric factor a of Eq. (61) with the diffusion constant and using the dimer scaling function (63), in all cases the results fit very well with the exact result given in Eq. (32) of Sec. III. This is shown in Fig. 11 (solid lines indicate the asymptotic solutions).

VII. SUMMARY AND OUTLOOK

We have considered the nonequilibrium behavior of stochastic systems involving processes of deposition and evaporation of k-mers on a one-dimensional substrate. Despite their apparent simplicity, these models exhibit a complex set of partially and fully jammed states belonging in turn to different subspaces disconnected by the dynamics. For $k \geq 2$ cooperative effects associated with the rule for deposition and evaporation induce a slow kinetics which can be detected by analyzing the power-law decays of dynamical correlation functions. For $k \geq 3$ exact enumeration algorithms support the hypothesis of proliferation of both fully and partially jammed steady states whose number grows exponentially with the number of lattice sites, indicating a nonergodic behavior in which the dynamics is partitioned in an equally exponentially large number of subspaces, a quite uncommon feature in systems without quenched disorder.

Starting from the master equation describing the kinetics of these processes, we have introduced a new class of quantum-spin Hamiltonians associated with the corresponding time evolution operators. The correspondence between these two types of problems enabled us to exploit global rotational symmetries of the spin Hamiltonian from which we derived a family of $k - 1$ independent conservation laws and conjectured important consequences for the asymptotic dynamical behavior. In the monomer case, these global symmetries do not apply and the kinetics is exponentially fast. For $k \geq 2$ continuous collective symmetries are always present and a slow dynamics can be inferred using the Goldstone theorem. The removal of this symmetry may cause drastic effects in the asymptotic dynamics, as was revealed by numerical simulations where the introduction of explicit particle diffusion or hopping processes changed the decay from power law to exponential.

The case $k = 2$ with equal deposition-evaporation rates is special in that it can be reduced to the isotropic Heisenberg ferromagnet and therefore an exact calculation of dynamical correlation functions showing diffusive decay is possible. The general dimer problem with unequal rates can be analyzed in terms of spin-wave descriptions, generalized particle diffusion and linear response approaches. Each of these methods yielded a diffusive dynamics also detected by Monte Carlo and finite-size scaling techniques. The case of $k \geq 3$ is more complex to solve by analytical methods except on some almost jammed subspaces. Nevertheless, Monte Carlo simulations on large scales and finite-size scaling analysis established again the existence of diffusive tails in the corresponding autocorrelation functions. Further, the data collapse of Fig. 8 strongly suggests the universality hypothesis of diffusive decay regardless of the value of k. The one apparent exception [Fig. 10(b)] is not at present understood.

In this work we have not investigated the behavior of static correlation functions. Studies in that direction are under consideration.

In view of the symmetry arguments discussed above, generalizations of this problem to include deposition and evaporation of $k_1, k_2, \ldots, k_n$ nearest-neighbor particles at a time could probably exhibit slow kinetics as well, provided that all k-mer sizes are chosen to be integer multiples of a common number, so that the continuous symmetry expressed in Eq. (53) remains unaltered in the generalized evolution operator. Such a system offers in addition the possibility of being numerically tractable on a linear chain.

Most of the ideas developed in this work can be extended to the general k-mer problem in higher dimensions. The case $k = 2$ with equal deposition-evaporation rates on the square lattice (and other bipartite lattices) can be mapped again to the Heisenberg ferromagnet. Furthermore, deposition and evaporation of lattice animals could also be considered within the formalism of Sec. V. For instance, square tetramers on a square substrate and elementary trimers on the sites of a triangular lattice have both collective continuous symmetries, and therefore at least one of the conditions for low lying Goldstone modes is fulfilled. However, trimers on the sites of a honeycomb lattice break this symmetry and one could speculate on the possibility of a fast kinetics. In general, the interplay between the animal shape and the underlying lattice structure is indeed a crucial feature to derive conclusions about the asymptotic dynamics.

ACKNOWLEDGMENTS

It is a pleasure to acknowledge fruitful discussions with V. Privman, B. Derrida, D. Dhar, and P. Thomas. We also thank J. W. Evans for sending us a copy of his review, before publication. We appreciate interesting remarks pointed out by A. Tsvelik, N. N. Chen, F. Alcaraz, J. Cardy, and D. Mattis. M.B. and M.D.G. are grateful to the Scientific and Engineering Research Council for financial support under Grant Nos. GR/G02741 and GR/G02727.

APPENDIX A: COVERAGE IN STEADY STATE FOR DIMERS

In the original dimer system, the coverage in steady state is defined as $\Theta_0 = (\langle N_A \rangle + \langle N_B \rangle)/L$ where $\langle N_A \rangle$, $\langle N_B \rangle$ are the average number of particles in equilibrium on the even and odd sites, respectively. In the τ-particle (sublattice-mapped) representation this becomes

$$\Theta_0 = \frac{1}{L}\left(\langle \tilde{N}_A \rangle + \left(\frac{L}{2} - \langle \tilde{N}_B \rangle\right)\right) = \frac{1}{2}\left(1 + \frac{\langle T_A \rangle - \langle T_B \rangle}{L}\right) \tag{A1}$$

where $\langle T_A \rangle$, $\langle T_B \rangle$ are the corresponding average sublattice magnetizations.

It is convenient to associate an energy

$$E(C) \equiv h\,\tilde{N}_B(C) - h\,\tilde{N}_A(C), \tag{A2}$$

to every configuration C. Corresponding Boltzmann weights $W(C) = e^{-E(C)/T}$ can then be attached to configurations. Comparing these weights with those corresponding to the steady state in Eq. (19), we find

$$\exp(2h/T) = \epsilon/\epsilon'. \tag{A3}$$

We consider the all-empty state in the original system. This corresponds to $\tilde{N}_A = 0$, $\tilde{N}_B = L/2$ in the sublattice representation. Since $\tilde{N}_A + \tilde{N}_B$ is conserved we restrict consideration to the sector with $L/2$ τ particles in it. The constraint $\tilde{N}_A + \tilde{N}_B = L/2$ can be enforced through a chemical potential μ. The corresponding grand partition function is

$$\mathcal{Z} = \sum_C \exp[\mu - E(C)]/T = (\mathcal{Z}_A)^{L/2}\,(\mathcal{Z}_B)^{L/2}, \tag{A4}$$

where

$$\mathcal{Z}_A = 1 + \exp\left(\frac{\mu + h}{T}\right)$$
$$\mathcal{Z}_B = 1 + \exp\left(\frac{\mu - h}{T}\right). \tag{A5}$$

The constraint $\langle \tilde{N}_A \rangle + \langle \tilde{N}_B \rangle = L/2$ yields $\mu = 0$, therefore we obtain

$$\langle \tilde{N}_A \rangle = \frac{L/2}{1 + \exp(-h/T)}, \quad \langle \tilde{N}_B \rangle = \frac{L/2}{1 + \exp(h/T)}. \tag{A6}$$

Thus, recalling (A1) and (A3), the coverage in steady state with zero total magnetization is

$$\Theta_0 = \frac{1}{1 + \sqrt{\epsilon'/\epsilon}}. \tag{A7}$$

APPENDIX B: CALCULATION OF AUTOCORRELATION FUNCTION FOR DIMERS ($\epsilon = \epsilon'$)

Since the particle occupation number n_i of site i is related to the spin by $n_i = (1+\tau_i^z)/2$, the autocorrelation function $C_{i,j}(t) = \langle n_i(t)\, n_j(0) \rangle - \langle n_i \rangle \langle n_j \rangle$ satisfies

$$C_{i,j}(t) = \tfrac{1}{4}[\langle \tau_i^z(t)\, \tau_j^z(0) \rangle - \langle \tau_i^z \rangle \langle \tau_j^z \rangle]. \tag{B1}$$

Then if $|k\rangle$ is the eigenvector of $\mathcal{H}$ with eigenvalue ε_k, and $|G_r\rangle$ is the ground state in the r-down spin sector, the correlation function in this sector is

$$C_{i,j}(t) = \frac{1}{4}\sum_k{}' \langle G_r | \tau_i^z | k \rangle \langle k | \tau_j^z | G_r \rangle \exp(-\epsilon_k t), \tag{B2}$$

where the prime on the sum indicates that $|k\rangle$ differs from $|G_r\rangle$.

The matrix elements have a selection rule arising from the fact that $\mathcal{H}$ commutes with the total spin $\hat{\mathbf{T}} = \frac{1}{2}\sum_i \hat{\tau}_i$, thus $\langle G_r | \tau_i^z | k \rangle = 0$ unless the total spin of $|k\rangle$ and $|G_r\rangle$ differ by 0 or 1. But $|G_r\rangle = B_r (T^-)^r |G_0\rangle$, where B_r is a normalization factor, $T^- \equiv \sum_i \tau_i^-$ and $|G_0\rangle$ is the all-spin-up state so $|G_r\rangle$ has total spin $T = L/2$. Further, $|k\rangle \neq |G_r\rangle$ so the states $|k\rangle$ which contribute have $T = L/2 - 1$. The state $|G_0\rangle$ (with no down spins) has $T = L/2$, $T^z = L/2$.

$T^-|G_0\rangle$ is the one-down-spin state having $T = L/2$. The other $(L-1)$ one-down-spin states having $T = L/2 - 1$ are simple spin-wave states $|q\rangle \equiv \sum_l \varphi_l(q)\,\tau_l^- |G_0\rangle$ with $\varphi_l(q) = L^{-1/2}\exp(iql)$ and energies $\varepsilon_q = 2\varepsilon(1 - \cos q)$.

The states $|k\rangle$ have $T = L/2 - 1$ but they have r-down spins. They are related to $|q\rangle$ by $|k\rangle = A_r (T^-)^{r-1} |q\rangle$. The normalization factor A_r is given by products of angular momentum factors $\sqrt{(T+T^z)(T-T^z+1)}$ with $T = L/2 - 1$ and T^z running from T downwards. Thus,

$$A_r = \sqrt{\frac{(L-r-1)!}{(L-2)!\,(r-1)!}}. \tag{B3}$$

Similarly, the normalization factor in $|G_r\rangle$ is

$$B_r = \sqrt{\frac{(L-r)!}{r!L!}}, \tag{B4}$$

hence

$$\langle G_r \,|\, \tau_i^z \,|\, k \rangle$$

$$= \sum_l \varphi_l(q)\, A_r\, B_r \,\langle G_0 \,|\, (T^+)^r\, \tau_i^z\, (T^-)^{r-1}\, \tau_l^- \,|\, G_0 \rangle\,,$$

$$= \varphi_i(q) \sqrt{\frac{r\,(L-r)}{L\,(L-1)}} \;\to\; \varphi_i(q)\, \sqrt{\tilde{\rho}\;(1-\tilde{\rho}\;)}\,, \qquad \text{(B5)}$$

where the last step involves the limit $r \to \infty$, $L \to \infty$ with r/L fixed at the particle density $\tilde{\rho}$. Thus

$$C_{i,j}(t) = \tilde{\rho}\;(1-\tilde{\rho}\;) \times \sum_{q \neq 0} \exp\left[-2\varepsilon\,(1-\cos q)\,t\right]\, \varphi_i(q)\, \varphi_j^*(q)\,. \qquad \text{(B6)}$$

The particular case $j = i$ (autocorrelation function) is therefore

$$C_{i,i}(t) = \tilde{\rho}\;(1-\tilde{\rho}\;)\, \exp(-2\varepsilon t)\, I_0(2\varepsilon t)\,, \qquad \text{(B7)}$$

$$I_0(z) \equiv \frac{1}{2\pi} \int_{-\pi}^{\pi} \exp(z\,\cos\theta)\, d\theta\,.$$

An alternative procedure for deriving these results for large L, r is to exploit the transformation of spin operators under rotations as follows. $|\, G_r \,\rangle$ is an eigenstate of $\mathcal{H}$, and of the square and z component of the total spin $\hat{\mathbf{T}}$. For large L, r the "vector" $\hat{\mathbf{T}}$ becomes classical, in the sense that its (normalized) components have commutators which vanish like $1/L$. Thus, if R is the operator which rotates all spins from the z direction by an angle θ (about the y axis, say), where $\cos\theta = 1 - 2r/L$, we have

$$|\, G_r \,\rangle = R\,|\, G_0 \,\rangle\,. \qquad \text{(B8)}$$

Thus

$$\langle k \,|\, \tau_j^z \,|\, G_r \,\rangle = \langle k \,|\, R\, R^{-1}\, \tau_j^z\, R \,|\, G_0 \,\rangle = \langle \tilde{k} \,|\, \left(\tau_j^z\, \cos\theta + \tau_j^x\, \sin\theta\right) \,|\, G_0 \,\rangle\,, \qquad \text{(B9)}$$

where $|\, \tilde{k} \,\rangle \equiv R^{-1}\,|\, k \,\rangle$ is again an eigenstate of $\mathcal{H}$, different from $|\, G_0 \,\rangle = R^{-1}\,|\, G_r \,\rangle$, because $[\mathcal{H},\, R] = 0$. Thus, using $\tau^x = (\tau^+ + \tau^-)$, $\tau^+\,|\, G_0 \,\rangle = 0$, $\tau^z\,|\, G_0 \,\rangle = |\, G_0 \,\rangle$, and the orthogonality of different eigenstates of $\mathcal{H}$, it follows that

$$\langle k \,|\, \tau_j^z \,|\, G_r \,\rangle = (\sin\theta)\langle \tilde{k} \,|\, \tau_j^- \,|\, G_0 \,\rangle = \frac{\sin\theta}{\sqrt{L}} \sum_q \exp\left(-iqj\right) \langle \tilde{k} \,|\, q \,\rangle\,, \qquad \text{(B10)}$$

where $|\, q \,\rangle$ is the single spin wave eigenstate with energy $\varepsilon_q = \varepsilon\,(1-\cos q)$. Inserting (B10) into (B2), and using orthonormality ($\langle \tilde{k} \,|\, q \,\rangle = \delta_{\tilde{k},q}$) and $\sin^2\theta = 4r\,(1 - r/L)/L = 4\,\tilde{\rho}\;(1-\tilde{\rho}\;)$, the results for $C_{i,j}(t)$, $C_{i,i}(t)$ in the limit $L \to \infty$, follow immediately.

APPENDIX C: THE NUMBER $I_1(k, L)$ OF FULLY JAMMED STATES

The fully jammed states have no more than $k-1$ successive parallel spins. In an open chain of L sites their number is

$$I_1(k, L) = \sum_{\alpha=1}^{k-1} M^\alpha(L)\,, \qquad \text{(C1)}$$

where $M^\alpha(L)$ is the number of fully jammed states with the last α spins parallel.

By adding an extra spin parallel or antiparallel to the last one,

$$M^\alpha(L+1) = M^{\alpha-1}(L) \;\;,\;\; k-1 \geq \alpha > 1\,, \qquad \text{(C2)}$$

$$M^1(L+1) = \sum_{\alpha=1}^{k-1} M^\alpha(L)\,. \qquad \text{(C3)}$$

Furthermore,

$$M^\alpha(1) = \begin{cases} 2, & \alpha = 1\,. \qquad \text{(C4)} \\ 0, & \alpha \neq 1\,. \qquad \text{(C5)} \end{cases}$$

(B2) implies

$$M^\alpha(L) = M^1(L-\alpha+1) \;\;,\;\; k-1 \geq \alpha \geq 1\,. \qquad \text{(C6)}$$

So all the other equations can be written in terms of $M^1(L)$. Or, equivalently, in terms of $I_1(k, L)$ since, by comparison of (C1) with (C3),

$$M^1(L) = I_1(k, L-1)\,. \qquad \text{(C7)}$$

The resulting equations take the following form in terms of

$$F_L(k) \equiv \tfrac{1}{2}\, I_1(k, L) \qquad \text{(C8)}$$

[which takes out the factor 2 from (C4)]:

$$F_L(k) = \sum_{j=1}^{k-1} F_{L-j}(k)\,, \qquad \text{(C9)}$$

with

$$F_0(k) = 1\,. \qquad \text{(C10)}$$

$$F_L(k) = 0 \;\;,\;\; -(k-2) \leq L < 0\,. \qquad \text{(C11)}$$

For the case $k = 2$, $F_L(k) = 1$, $L \geq 0$, so $I_1(2, L) = 2$. For the case $k = 3$, (C9)–(C11) are the defining equations of Fibonacci numbers F_n, so $I_1(3, L) = 2\,F_L(3) = 2\,F_L$. For higher k, $F_L(k)$ are the "generalized Fibonacci numbers" defined by (C9)–(C11), general k.

By solving the linear difference equation (C9) it can be seen that in general $I_1(k, L) = 2\,F_L(k)$ is at large L

proportional to λ^L where λ is the largest root of

$$\lambda^k = 2\lambda^{k-1} - 1 . \tag{C12}$$

APPENDIX D: RANDOM WALK OF SPIN FLIPS ON THE FULLY JAMMED TRIMER ANTIFERROMAGNETIC STATE

The fully jammed antiferromagnetic state of the trimer system is $|\varphi\rangle = (\uparrow\downarrow)^{L/2} \equiv \uparrow\downarrow\uparrow\downarrow \ldots$. Taking the origin $n = 0$ at an up spin state, we consider an initial state $|a_0\rangle \equiv \sigma^-_{n=0}|\varphi\rangle$. This state is a three-down-spin group centered at the origin, separating two antiferromagnetic domains of opposite registration. Repeated application of the trimer Hamiltonian produces a sequence of states $\ldots|a_m\rangle, |b_m\rangle \ldots$ as follows:

$$\begin{aligned} |a_0\rangle &= \hat{\beta}\,|b_0\rangle , \\ |b_0\rangle &= \hat{\gamma}\,\left(|a_0\rangle + |a_1\rangle + |a_1\rangle^\dagger\right) , \\ |a_m\rangle &= \hat{\alpha}\,\left(|b_m\rangle + |b_{m-1}\rangle\right) \ , \ m \geq 1 , \\ |b_m\rangle &= \hat{\alpha}'\,\left(|a_m\rangle + |a_{m+1}\rangle\right) \ , \ m \geq 1 , \end{aligned} \tag{D1}$$

where

$$\begin{aligned} \hat{\alpha}(H) &= \epsilon\,(H + 2\epsilon)^{-1} , \\ \hat{\alpha}'(H) &= \epsilon'\,(H + 2\epsilon')^{-1} , \\ \hat{\beta}(H) &= \epsilon\,(H + \epsilon)^{-1} , \\ \hat{\gamma}(H) &= \epsilon'\,(H + 3\epsilon')^{-1} . \end{aligned} \tag{D2}$$

The generalized states $|a_m\rangle, |b_m\rangle$ have a group of three down spins or three up spins, respectively, which are $2m$ lattice spacings to the left of the origin. The "dagger" symbol in $|a_1\rangle^\dagger$ represents reflection in the origin. The time evolution is thus a generalized random walk, in this case of the "three-groups" on the antiferromagnetic background. Eigensolutions of the form $|a_m\rangle \propto a\exp(i2mq), |b_m\rangle \propto b\exp(i2mq)$ yield the secular equation

$$(2\cos q)^2\,\hat{\alpha}(E)\,\hat{\alpha}'(E) = 1 . \tag{D3}$$

It follows that the eigenenergy satisfies

$$E_q^2 - 2E_q(\epsilon + \epsilon') + 4\epsilon\epsilon'\sin^2 q = 0 . \tag{D4}$$

[1] For recent reviews see, e.g. M. C. Bartelt and V. Privman, Int. J. Mod. Phys. B **5**, 2883 (1991); J. W. Evans (unpublished).

[2] P. J. Flory, J. Am. Chem. Soc. **61**, 1518 (1939).

[3] R. Dickman and R. Burschka, Phys. Lett. A **127**, 132 (1988).

[4] A. H. Bretag, B. R. Davis, and D. I. B. Kerr, J. Membr. Biol. **16**, 363 (1974).

[5] A. H. Bretag, C. A. Hurst, and D. I. B. Kerr, J. Chem. Biol. **73**, 367 (1978).

[6] R. M. Ziff, E. Gulari, and Y. Barshad, Phys. Rev. Lett. **56**, 2553 (1988).

[7] D. Ben-Avraham and J. Kohler, J. Stat. Phys. **65**, 839 (1991); E. Clement, P. Leroux-Hugon, and L. M. Sander, Phys. Rev. Lett. **67**, 1661 (1991); P. L. Krapivsky, Phys. Rev. A **45**, 1067 (1992).

[8] T. Moriya, in *Magnetism*, edited by G. T. Rado and H. Suhl (Academic, New York, 1963), Vol. 1.

[9] J. Goldstone, A. Salam, and S. Weinberg, Phys. Rev. **127**, 965 (1962); for fuller accounts see, e.g., S. Abers and B. W. Lee, Phys. Rep. **9**, 1 (1973) and N. N. Bogoliubov, *Lectures in Statistical Physics, Vol. 2* (Gordon and Breach, London, 1970).

[10] M. Barma, M. D. Grynberg, and R. B. Stinchcombe, Phys. Rev. Lett. **70**, 1033 (1993).

[11] N. G. van Kampen, *Stochastic Processes in Physics and Chemistry* (North-Holland, Amsterdam, 1981).

[12] H. N. V. Temperley and E. H. Lieb, Proc. R. Soc. London Ser. A **322**, 251 (1971); R. J. Baxter, *Exactly Solved Models in Statistical Mechanics* (Academic, London, 1982).

[13] J. W. Evans and C. A. Hurst, Phys. Rev. A **40**, 3461 (1989).

[14] E. R. Cohen and H. Reiss, J. Chem. Phys. **38**, 680 (1963).

[15] D. Dhar, P. Thomas, and M. Barma (unpublished).

[16] E. T. Whittaker and G. N. Watson, *A Course of Modern Analysis* (Cambridge University Press, Cambridge, England, 1969), p. 464.